Research Article

SURFACE and INTERFACE ANALYSIS

Received: 22 December 2009 Revised: 18 March 2010 Accepted: 31 March 2010 Published online in Wiley Online Library: 4 August 2010

(wileyonlinelibrary.com) DOI 10.1002/sia.3522

Calculations of electron inelastic mean free paths. IX. Data for 41 elemental solids over the 50 eV to 30 keV range

S. Tanuma,[a] C. J. Powell[b]* and D. R. Penn[b]

We have calculated inelastic mean free paths (IMFPs) for 41 elemental solids (Li, Be, graphite, diamond, glassy C, Na, Mg, Al, Si, K, Sc, Ti, V, Cr, Fe, Co, Ni, Cu, Ge, Y, Nb, Mo, Ru, Rh, Pd, Ag, In, Sn, Cs, Gd, Tb, Dy, Hf, Ta, W, Re, Os, Ir, Pt, Au and Bi) for electron energies from 50 eV to 30 keV. The IMFPs were calculated from experimental optical data using the full Penn algorithm for energies up to 300 eV and the simpler single-pole approximation for higher energies. The calculated IMFPs could be fitted to a modified form of the Bethe equation for inelastic scattering of electrons in matter for energies from 50 eV to 30 keV. The average root-mean-square (RMS) deviation in these fits was 0.48%. The new IMFPs were also compared with IMFPs from the predictive TPP-2M equation; in these comparisons, the average RMS deviation was 12.3% for energies between 50 eV and 30 keV. This RMS deviation is almost the same as that found previously in a similar comparison for the 50 eV – 2 keV range. Relatively large RMS deviations were found for diamond, graphite and cesium. If these three elements were excluded in the comparison, the average RMS deviation was 9.2% between 50 eV and 30 keV. We found satisfactory agreement of our calculated IMFPs with IMFPs from recent calculations and from elastic-peak electron-spectroscopy experiments.

Keywords: Inelastic mean free paths; Elemental solids; AES; XPS

Introduction

Data for elastic and inelastic scattering of electron in solids are needed for determining the surface sensitivity of electron spectroscopies such as Auger-electron spectroscopy (AES) and XPS and for quantitative analyses with these techniques.[1,2] The inelastic mean free path (IMFP) is the key material parameter that has been used to describe inelastic scattering of the detected signal electrons in AES and XPS as well as of the primary electrons in AES.

We have previously reported calculations of IMFPs of 50 – 2000 eV electrons from experimental optical data for 41 elemental solids, 15 inorganic compounds and 14 organic compounds, as well as analyses of these results.[3,4,5,6,7,8,9,10] The optical data were checked for internal consistency using two sum rules;[11] these checks indicated that the optical data for the group of elemental solids and the group of organic compounds were more reliable than those for the group of inorganic compounds. We analyzed IMFPs for the groups of elemental solids and organic compounds to derive an equation, designated TPP-2M,[7] based on the Bethe equation[12] for inelastic scattering of electrons in matter. We found that the four parameters in the TPP-2M equation could be empirically related to several material parameters (atomic or molecular weight, density, number of valence electrons per atom or molecule, and the bandgap energy for nonconductors). The TPP-2M equation could then be used to estimate IMFPs for other materials over the 50 – 2 000 eV energy range, the range of practical interest for most AES measurements and for XPS performed with Al or Mg Kα X-ray sources.

In recent years, there has been growing interest in XPS and related experiments performed with X-rays of much higher energies for both scientific and technological purposes. So-called hard XPS is being applied with X-rays from synchrotron-light sources (with energies up to 15 keV) and with Cu Kα X-ray sources (with an energy of 8.048 keV) to characterize film composition and buried interfaces of multilayer thin-film samples and powders.[13,14,15] In these applications, the higher X-ray energies were needed to enable sample characterizations without removal of surface layers by ion sputtering. We therefore have extended our earlier work by calculating IMFPs for 41 elemental solids (Li, Be, graphite, diamond, glassy C, Na, Mg, Al, Si, K, Sc, Ti, V, Cr, Fe, Co, Ni, Cu, Ge, Y, Nb, Mo, Ru, Rh, Pd, Ag, In, Sn, Cs, Gd, Tb, Dy, Hf, Ta, W, Re, Os, Ir, Pt, Au and Bi) and for electron energies from 50 eV to 30 keV.

We briefly describe our IMFP algorithm and the sources of optical data we have used, present the new IMFP results, analyze the degree of consistency of IMFPs from the TPP-2M equation with the new IMFPs over the 50 eV – 30 keV range, and compare the new IMFPs with values from recent calculations and from elastic-peak electron spectroscopy (EPES).[16,17] We conclude with a summary.

IMFP Calculations

Our method for IMFP calculations from experimental optical data has been described previously.[3,4] We make use of the Penn algorithm[18] which is expected to give reasonable results for electron energies above 50 eV.[4] IMFPs were calculated at

* *Correspondence to: C. J. Powell, National Institute of Standards and Technology, Gaithersburg, MD 20899, USA. E-mail: cedric.powell@nist.gov*

a *National Institute for Materials Science, 1-2-1 Sengen, Tsukuba, Ibaraki 305-0047, Japan*

b *National Institute of Standards and Technology, Gaithersburg, MD 20899, USA*

equal energy intervals on a logarithmic scale corresponding to increments of 10% from 10 eV to 30 keV. We first give a summary of our implementation of the Penn algorithm and then describe the checks we made of the optical data.

The IMFP λ for an electron of energy $E_k = \hbar^2k^2/2m$ in solids can be expressed as

$$\lambda = \left(\frac{\hbar k}{m}\right)\left[\frac{\hbar}{2|M_l(k)|}\right], \quad (1)$$

where $\hbar k/m$ is the electron velocity and $2M_l/\hbar$ is its inverse lifetime due to inelastic-scattering processes.[18,19]

For electron energies between 10 eV and 300 eV, we calculated $M_l(k)$ using the full Penn algorithm (FPA):

$$M_l(k) = \int_0^\infty d\omega_p G(\omega_p)\left[\frac{1}{\pi a_0 k}\int_0^{E_k-E_F} d(\hbar\omega)\int_{q-}^{q+}\frac{dq}{q}\mathrm{Im}\left[\frac{1}{\varepsilon_L(q,\omega;\omega_p)}\right]\right] \quad (2a)$$

$$q\pm = k\left\{1 \pm \left[1-(\hbar\omega/E_k)\right]^{0.5}\right\} \quad (2b)$$

$$G(\omega) = -\frac{2}{\pi\omega}\mathrm{Im}\frac{1}{\varepsilon(\omega)}, \quad (2c)$$

where a_0 is the Bohr radius, ε_L is the Lindhard model dielectric function,[20] $\varepsilon(\omega)$ is the optical dielectric function, E_F is the Fermi energy, ω is the frequency, q is the momentum transfer, and ω_p is the free-electron plasmon frequency.

For energies from 330 eV to 30 keV, we used the simpler single-pole approximation (SPA) or simple Penn algorithm to calculate $M_l(k)$. In this approximation,

$$\mathrm{Im}\left[\frac{1}{\varepsilon_L(q,\omega;\omega_p)}\right] = -\frac{\pi}{2}\frac{\omega_P^2}{\omega_P(q)}\delta(\omega-\omega_P(q)) \quad (3a)$$

$$\omega_P^2(q) = \omega_P^2 + \frac{1}{3}[v_F(\omega_P)q]^2 + \left(\frac{\hbar q^2}{2m}\right)^2, \quad (3b)$$

where $v_F(\omega_P)$ is the Fermi velocity of a free-electron gas with plasmon frequency equal to ω_p. From Eqns (2) and (3), $M_l(k)$ in the SPA can be expressed as

$$M_l(k) = \frac{1}{2\pi a_0 k}\int d(\hbar\omega_P)\mathrm{Im}\frac{1}{\varepsilon(\omega_P)}\ln\left[\frac{\overline{\omega}_P+\overline{\omega}_P(q)}{\overline{q}^2}+\frac{2}{3\overline{\omega}_P}\right]_{\overline{q}_2}^{\overline{q}_1}, \quad (4)$$

where $\overline{\omega}_P = \hbar\omega_P/E_F$, $\overline{q} = q/k_F$, and $\omega_P(q)^2 = \overline{\omega}_P^2 + 4\overline{q}^2/3 + \overline{q}^4$. Analytical expressions for $\overline{q}_1$ and $\overline{q}_2$ are given in Appendix A of Ref. [18].

We note that the difference in IMFPs obtained using these two algorithms at 300 eV is very small (e.g. <0.2% for graphite). We also point out that we used the FPA in our previous IMFP calculations for energies less than 200 eV.[4,5,7,10]

We show IMFPs for energies between 10 and 50 eV in the figures below to indicate IMFP trends vs electron energy; these results should be considered only as rough estimates. All kinetic energies are expressed with respect to the Fermi level.

Table 1 contains material-property data used in the IMFP calculations or in the later analysis of the IMFP results. We show values of the atomic weight M, bulk density ρ (g cm^{-3}), number of valence electrons per atom (N_v),[7] free-electron plasmon energy ($E_P = 28.8(N_v\rho/M)^{1/2}$ eV), bandgap energy (E_g), and Fermi energy (E_F), a parameter used in the IMFP calculations.

Table 1. Values of material parameters used in the IMFP calculations and for the analysis of IMFP results for the indicated elemental solids

Element	M	ρ (g cm^{-3})	N_v	E_p (eV)	E_g (eV)	E_F (eV)
Li	6.941	0.534	1.0	7.99	0	4.74
Be	9.01218	1.848	2.0	18.44	0	14.3
C (graphite)	12.011	2.25	4.0	24.93	0	20.4
C (diamond)	12.011	3.515	4.0	31.16	5.5	20.4
C (glassy)	12.011	1.8	4.0	22.30	0	20.4
Na	22.989768	0.971	1.0	5.92	0	3.24
Mg	24.3050	1.738	2.0	10.89	0	7.1
Al	26.98154	2.7	3.0	15.78	0	11.2
Si	28.0855	2.33	4.0	16.59	1.1	12.5
K	39.0983	0.862	1.0	4.28	0	2.12
Sc	44.95591	2.989	3.0	12.86	0	5.8
Ti	47.867	4.51	4.0	17.68	0	6.0
V	50.942	6.11	5.0	22.30	0	6.4
Cr	51.9961	7.14	6.0	26.14	0	7.8
Fe	55.845	7.874	8.0	30.59	0	8.9
Co	58.9332	8.90	9.0	33.58	0	10
Ni	58.6934	8.902	10.0	35.47	0	9.1
Cu	63.546	8.96	11.0	35.87	0	8.7
Ge	72.59	5.32	4.0	15.59	0.67	12.6
Y	88.906	4.469	3.0	11.18	0	4.4
Nb	92.90638	8.57	5.0	19.56	0	5.3
Mo	95.94	10.28	6.0	23.09	0	6.5
Ru	101.07	12.41	8.0	28.54	0	6.9
Rh	102.90550	12.41	9.0	30.00	0	6.9
Pd	106.42	12.02	10.0	30.61	0	6.2
Ag	107.8682	10.5	11.0	29.80	0	7.2
In	114.818	7.31	3.0	12.59	0	4.82
Sn	118.71	7.31	4.0	14.29	0	5.51
Cs	132.90543	1.88	1.0	3.43	0	1.73
Gd	157.25	8.23	9.0	19.77	0	3.5
Tb	158.92534	8.25	9.0	19.69	0	4.0
Dy	162.5	8.78	9.0	20.08	0	3.5
Hf	178.49	13.31	4.0	15.73	0	7.9
Ta	180.9479	16.65	5.0	19.53	0	8.4
W	183.85	19.3	6.0	22.86	0	10.1
Re	186.207	21.02	7.0	25.60	0	10.7
Os	190.23	22.61	8.0	28.08	0	11.4
Ir	192.217	22.65	9.0	29.66	0	11.2
Pt	195.08	21.45	10.0	30.20	0	10.6
Au	196.967	19.32	11.0	29.92	0	9.0
Bi	208.98037	9.79	5.0	13.94	0	12.6

IMFPs were calculated from energy-loss functions (ELFs) that were obtained from experimental optical data or ELF measurements for each elemental solid. The sources of ELF data are listed in Table 2 for 25 of our solids;[21,22,23,24,25,26,27,28,29,30,31] ELF sources for the other 16 solids are shown in Table 2 of Ref. [10]. Since no direct measurements of optical constants were available for photon energies larger than about 50 eV for most of the solids, it was necessary to make use of atomic photoabsorption data for photon energies beyond the particular measurement range. This use of atomic data is not considered a serious source of error because the complex dielectric constant, $\varepsilon(\omega)$, as a function of frequency, ω, for photon energies larger than about 50 eV is mainly determined by atomic properties except in the vicinity

SURFACE and INTERFACE ANALYSIS

Table 2. Sources of optical data and energy-loss function measurements used in the IMFP calculations for 25 of the elemental solids considered here

Element	Photon energy range (eV)	Source of data
Mg	1–600	Ref. [21]
	609.43–30 000	Ref. [22]
Si	0.005–2 000	Ref. [23]
	2 025.3–30 000	Ref. [22]
Ti	1–54	Ref. [27]
	56–88	Interpolation of ELF data with an $a + b/(E - c)^d$ equation
	91.623–30 000	Ref. [22]
V	0.1–24	Ref. [30]
	24.55–40	Ref. [26]
	42.5–120	Ref. [30]
	122.88–30 000	Ref. [22]
Cr	0.04–29.52	Ref. [26]
	30–35	Interpolation of ELF data with a quartic equation
	36.003–30 000	Ref. [22]
Fe	0.1–30	Ref. [26]
	31–45	Interpolation of ELF data with a quartic equation
	41.778–30 000	Ref. [22]
Co	0.5–70.5	Ref. [27]
	72.059–30 000	Ref. [22]
Ni	0.1–2 000	Ref. [23]
	2 025.3–30 000	Ref. [22]
Cu	1–95	Ref. [21]
	101.94–30 000	Ref. [22]
Y	0.1–39.5	Ref. [31]
	40.059–30 000	Ref. [22]
Nb	0.12–40.5	Ref. [26]
	41.143–30 0000	Ref. [22]
Mo	0.1–30	Ref. [23]
	31–39	Interpolation of ELF data with a cubic equation
	40.059–30 000	Ref. [22]
Ru	0.1–40	Ref. [26]
	41.3–50.6	Ref. [24]
	52.312–30 000	Ref. [22]
Rh	0.1–40	Ref. [23]
	41.143–30 000	Ref. [22]
Pd	0.1–17.26	Ref. [30]
	18–120	Interpolation of ELF data with a cubic spline function
	122.88–30 000	Ref. [22]
Ag	1–30 000	Ref. [21]
Hf	0.52–24.8	Ref. [26]
	26–50	Interpolation of ELF data with a quintic equation
	50.935–30 000	Ref. [22]
Ta	0.1–35	Ref. [30]
	36–46	Interpolation of ELF data with a quartic equation
	47.016–30 000	Ref. [22]
W	0.05–33.5	Ref. [23]
	34–39	Interpolation of ELF data with a cubic spline function
	40.059–30 000	Ref. [22]
Re	0.1–37	Ref. [26]
	38–43	Interpolation of ELF data with a quartic equation
	43.398–30 000	Ref. [22]
Os	0.1–39	Ref. [23]
	40.059–30 000	Ref. [22]
Ir	0.1–40	Ref. [23]
	41.143–30 000	Ref. [22]
Pt	0.1–82.66	Ref. [23]
	84–98	Interpolation of ELF data with a cubic equation
	100–2000	Ref. [28]
	2025.3–30 000	Ref. [22]
Au	0.1–9919	Ref. [23]
	10 044–30 000	Ref. [22]
Bi	0.6–30 000	Ref. [21]

of core-electron excitation thresholds. The latter differences are unimportant in the IMFP calculation because integration is made of the energy-loss function over $\hbar\omega$. In addition, the ELF $\mathrm{Im}[-1/\varepsilon(\omega)] \approx \mathrm{Im}[\varepsilon(\omega)]$ for photon energies above about 50 eV, and $\mathrm{Im}[\varepsilon(\omega)]$ can be obtained easily from photoabsorption cross-sections. We point out we have made use of photoabsorption data for 22 solids (Mg, Ti, V, Cr, Fe, Co, Ni, Y, Nb, Mo, Ru, Rh, Pd, Hf, Ta, W, Re, Os, Ir, Pt and Au) from Henke *et al*.[22] that is more recent than the data used for our previous IMFP calculations.[3,4] For some of these solids (Cr, Fe, Mo, Hf, Ta, W, Re and Pt), it was necessary to make interpolations between two energy-loss regions, and we were guided in this process by measured transmission and reflection electron energy-loss spectroscopy (REELS) data.[30–34] The resulting ELFs were in better agreement overall with the energy-loss data[30,32,33,34,35] and resulted in smaller sum-rule errors (described below) for most of the solids than for our earlier IMFP work.[3,4] For Co, we selected optical data from a recent analysis of REELS data by Werner *et al*.[27] for energy losses up to 70.5 eV because the resulting ELF was in much better agreement with the ELF from transmission electron energy-loss experiments[34] than with the ELF obtained from optical experiments;[30] the sum-rule errors were also appreciably smaller. A similar choice was made for Ti where there was improved agreement of the new ELF with the REELS data of Robins and Swan.[32] Finally, we have chosen a set of optical data from Palik[23] for gold since this dataset gave an ELF in better agreement with transmission electron energy-loss experiments[36] than the dataset from Hagemann *et al*.[21] that we used previously.[3,4] We will later make comparisons of the IMFPs from the newer optical data with the IMFPs that we reported earlier.

We checked the internal consistency of the ELF data through use of the oscillator-strength sum rule (or f-sum rule) and a limiting form of the Kramers–Kronig integral (or KK-sum rule).[5,11] The f-sum can be evaluated as the total effective number of electrons per atom, Z_{eff}, contributing to the inelastic scattering:

$$Z_{eff} = (2/\pi\hbar^2\Omega_p^2)\int_0^{\Delta E_{\max}} \Delta E\,\mathrm{Im}[-1/\varepsilon(\Delta E)]d(\Delta E), \qquad (5)$$

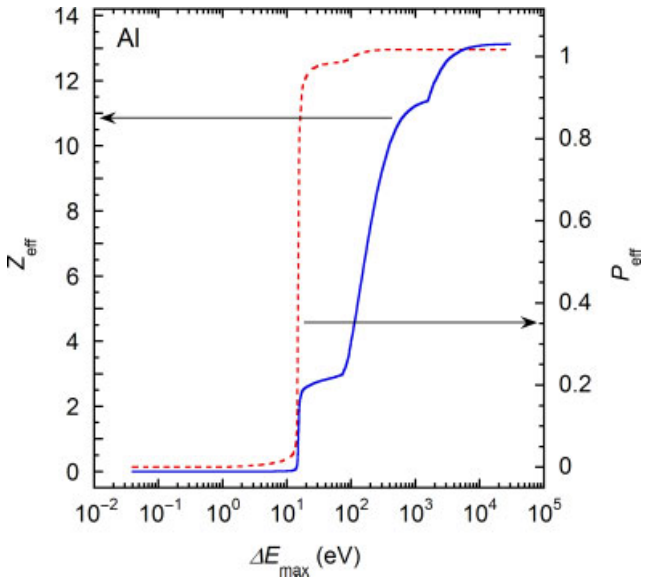

Figure 1. Plots of Z_{eff} from Eqn (5) (solid line) and P_{eff} from Eqn (6) (short-dashed line) as a function of ΔE_{max} for aluminum.

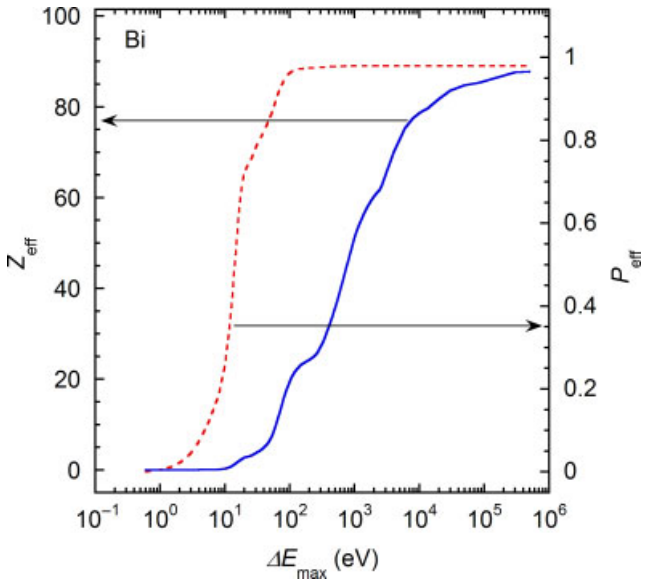

Figure 2. Plots of Z_{eff} from Eqn (5) (solid line) and P_{eff} from Eqn (6) (short-dashed line) as a function of ΔE_{max} for bismuth.

where $\Delta E = \hbar\omega$, $\Omega_P = (4\pi n_a e^2/m)^{1/2}$, $n_a = N_a\rho/M$ is the density of atoms, and N_a is Avogadro's number. When the upper limit ΔE_{max} in Eqn (5) is equal to infinity, Z_{eff} should be equal to Z, the total number of electrons per atom. The KK-sum can be expressed as:

$$P_{eff} = (2/\pi)\int_0^{\Delta E_{max}} \Delta E^{-1}\mathrm{Im}[-1/\varepsilon(\Delta E)]d(\Delta E) + n^{-2}(0), \qquad (6)$$

where $n(0)$ is the limiting value of the refractive index at low photon energies (below those where absorption maxima are observed). In the limit $\Delta E_{max} \to \infty$, $P_{eff} \to 1$. We determined Z_{eff} and P_{eff} from Eqns (5) and (6) for each solid as a function of ΔE_{max} up to a maximum value of 30 keV. For $Z > 50$ (Sn), we expect Z_{eff} to be less than Z because K-shell excitations cannot contribute to the integral of Eqn (5) when ΔE_{max} is 30 keV (i.e. the K-shell binding energy of Sn is 29.2 keV and that of Sb is 30.5 keV). Although there are two electrons in the K shell, the contributions of these electrons to the f-sum will be less than 2.[12] We have compared our evaluations of Z_{eff} for elements with $Z \geq 50$ with $Z - 1.65$ since the average contribution of K-shell excitations to the f-sum integrals for four low-Z elements (Na, Al, K and Sc) was 1.65.[10]

As examples, Figs. 1 and 2 show plots of Z_{eff} and P_{eff} as a function of ΔE_{max} for Al and Bi. The maximum values of Z_{eff} for each solid are in very good agreement with the expected values (Z for Al and $Z - 1.65$ for Bi), and the maximum values of P_{eff} are similarly very close to the expected value (unity). For each element, the differences are less than 3%. Table 3 lists errors in the f-sum and KK-sum rules for each elemental solid, that is, the differences between the computed values of Z_{eff} and P_{eff} and those expected from Eqn (5) (Z or $Z - 1.65$) and Eqn (6). The average root-mean-square (RMS) errors for the sets of ELF data based on the f-sum rule and KK-sum rules are 4.2 and 7.7%, respectively.

Figure 3 shows the relation between f-sum- and KK-sum-rule errors. We see from Fig. 3 and Table 3 that there is one solid for which the f-sum-rule error is slightly larger than 10% (Mg) and six solids for which the KK-sum-rule error is larger than 10% (K, Nb, Rh, Pd, Sn and Pt). Of these seven solids, the sum-rule errors for K and Nb are both of the same sign (negative in each case),

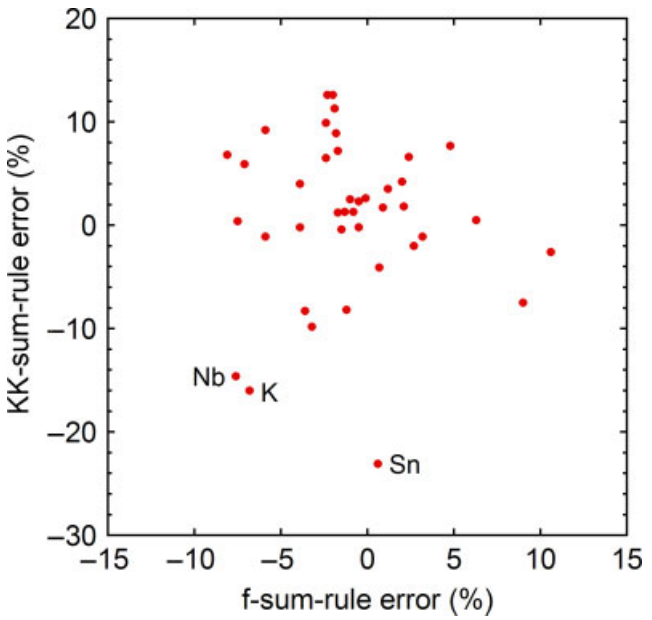

Figure 3. Plot of errors of KK- sum rule [Eqn (6)] versus errors of f-sum rule [Eqn (5)] for the 41 elemental solids.

indicating that their ELFs are systematically too small and, thus, their calculated IMFPs will be too large. For 34 of our 41 elemental solids, the f-sum-rule and KK-sum rule errors are both less than 10%.

IMFP Results

Table 4 shows IMFPs calculated from optical data for our 41 elemental solids for electron energies between 50 eV and 30 keV. Plots of the calculated IMFPs as a function of energy are shown as solid circles in Figs. 4–10. IMFPs are included in these plots for energies less than 50 eV to illustrate trends, but these data are not

SURFACE and INTERFACE ANALYSIS

Table 3. List of elemental solids with values of Z or $Z-1.65$ (in text), Z_{eff} from Eqn (5), errors in the f-sum rule, values of P_{eff} from Eqn (6), and errors in the KK-sum rule. Values of Z_{eff} and P_{eff} were determined with $\Delta E_{max} = 30$ keV

Element	Z or $Z-1.65$	Z_{eff}	Error in f-sum rule (%)	P_{eff}	Error in KK-sum rule (%)
Li	3	3.06	2.1	1.018	1.8
Be	4	4.09	2.4	1.066	6.6
C (graphite)	6	6.29	4.8	1.077	7.7
C (diamond)	6	5.97	−0.5	0.998	−0.2
C (glassy)	6	5.77	−3.9	0.998	−0.2
Na	11	11.13	1.2	1.035	3.5
Mg	12	13.28	10.6	0.974	−2.6
Al	13	13.12	0.9	1.017	1.7
Si	14	14.10	0.7	0.959	−4.1
K	19	17.72	−6.8	0.840	−16.0
Sc	21	22.90	9.0	0.925	−7.5
Ti	22	21.90	−0.5	1.023	2.3
V	23	22.81	−0.8	1.013	1.3
Cr	24	22.30	−7.1	1.059	5.9
Fe	26	23.90	−8.1	1.068	6.8
Co	27	26.55	−1.7	1.012	1.2
Ni	28	27.32	−2.4	1.065	6.5
Cu	29	28.55	−1.5	0.996	−0.4
Ge	32	32.65	2.0	1.042	4.2
Y	39	37.76	−3.2	0.902	−9.8
Nb	41	37.90	−7.6	0.854	−14.6
Mo	42	39.53	−5.9	0.989	−1.1
Ru	44	41.43	−5.9	1.092	9.2
Rh	45	44.11	−2.0	1.126	12.6
Pd	46	44.94	−2.3	1.126	12.6
Ag	47	49.97	6.3	1.005	0.5
In	49	47.25	−3.6	0.917	−8.3
Sn	48.35	48.64	0.6	0.769	−23.1
Cs	53.35	49.33	−7.5	1.004	0.4
Gd	62.35	62.27	−0.1	1.026	2.6
Tb	63.35	64.89	2.4	1.066	6.6
Dy	64.35	66.42	3.2	0.989	−1.1
Hf	70.35	69.50	−1.2	0.918	−8.2
Ta	71.35	70.65	−1.0	1.025	2.5
W	72.35	71.39	−1.3	1.013	1.3
Re	73.35	72.10	−1.7	1.072	7.2
Os	74.35	71.42	−3.9	1.040	4.0
Ir	75.35	73.55	−2.4	1.099	9.9
Pt	76.35	74.87	−1.9	1.113	11.3
Au	77.35	75.99	−1.8	1.089	8.9
Bi	81.35	83.58	2.7	0.980	−2.0

considered reliable.[4] Sources of uncertainties of the calculated IMFPs are discussed elsewhere.[1,6,16,37,38,39] The uncertainties of IMFPs for energies between 50 and 200 eV are expected to be larger than those for higher energies.[16] Further comments on uncertainties of IMFPs for energies less than 200 eV are given in the Discussion section where we also make comparisons of our calculated IMFPs with those reported by several other groups.

The plots of the calculated IMFPs in Figs 4–10 show similar dependences on electron energy for energies greater than 200 eV. For lower energies, however, different dependences were found. The latter differences are associated with the different electronic properties and thus ELFs of each material.[40]

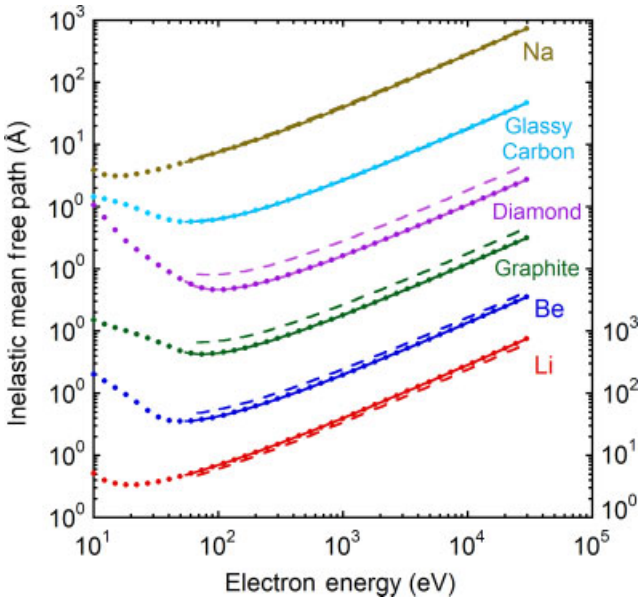

Figure 4. Plots of electron inelastic mean free paths as a function of electron energy for Li, Be, graphite, diamond, glassy carbon and Na. The solid circles show calculated IMFPs from the Penn algorithm (Table 4). The solid lines show fits to these IMFPs with the modified Bethe equation [Eqn (7)] and the derived parameters in Table 5. The long-dashed lines indicate IMFPs calculated from the TPP-2M equation [Eqns (7) and (13)]. The ordinate scale on the right indicates the IMFP scale for Li. Successive plots have been displaced vertically for clarity, and the ordinate scale at the left indicates these displacements.

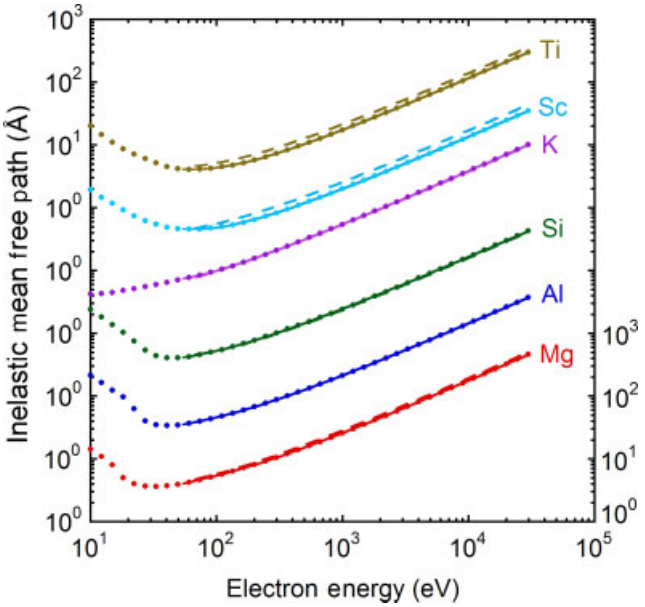

Figure 5. Plots of electron inelastic mean free paths as a function of electron energy for Mg, Al, Si, K, Sc and Ti. See caption to Fig. 4.

Figure 11 shows plots of the ratio of the IMFPs in Table 4 for 18 of the 22 elements with the newer ELFs that we used here (λ_{new}) to the corresponding IMFPs that we published previously[4] (λ_{old}). For the remaining four elements (Mg, Co, Ni and Pt), the IMFP changes were less than 1%. For 10 of the 18 solids in Fig. 11, the IMFPs are smaller than the earlier values at an energy of 99.5 eV, while at 992 eV the IMFPs are smaller for 11 of the solids.

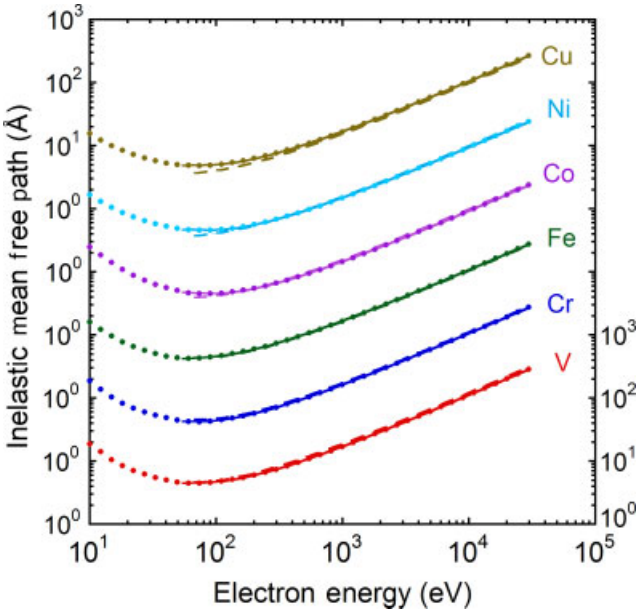

Figure 6. Plots of electron inelastic mean free paths as a function of electron energy for V, Cr, Fe, Co, Ni and Cu. See caption to Fig. 4.

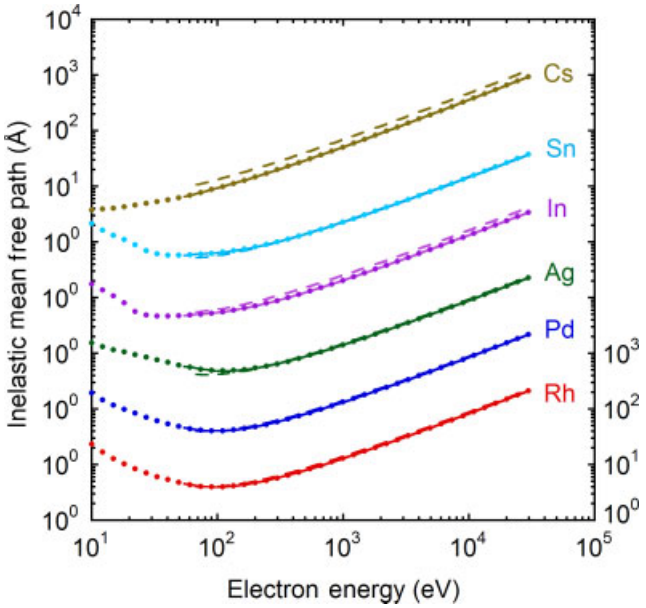

Figure 8. Plots of electron inelastic mean free paths as a function of electron energy for Rh, Pd, Ag, In, Sn and Cs. See caption to Fig. 4.

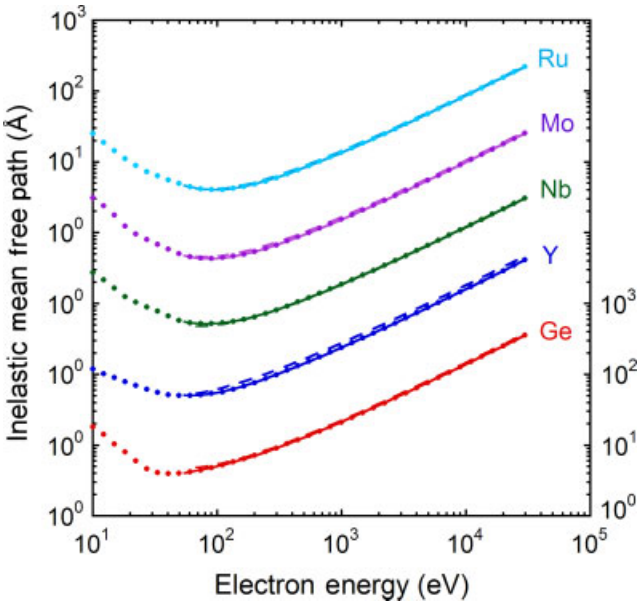

Figure 7. Plots of electron inelastic mean free paths as a function of electron energy for Ge, Y, Nb, Mo and Ru. See caption to Fig. 4.

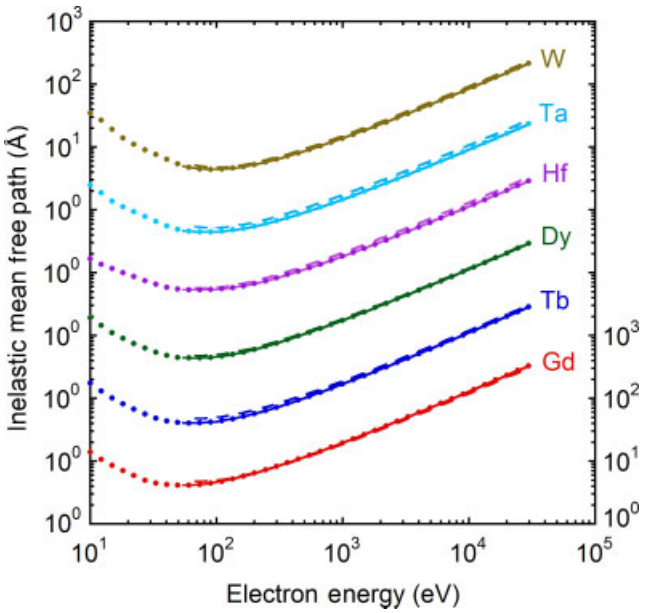

Figure 9. Plots of electron inelastic mean free paths as a function of electron energy for Gd, Tb, Dy, Hf, Ta and W. See caption to Fig. 4.

The largest changes occurred for Pd (a decrease) and for Re (an increase). While the ratios are nearly constant for energies above about 300 eV, different energy dependences are seen for lower energies. The various magnitudes of the ratios in Fig. 11 and the different energy dependences are associated with the new ELFs that we adopted for the present IMFP calculations. The new IMFPs are believed to be more reliable because of the smaller sum-rule errors of the new ELFs compared to the sum-rule errors for our IMFPs published previously.[4]

In our previous work,[4,5,6,10] we analyzed the IMFP dependence on energy for each material with a modified form of the Bethe equation for inelastic electron scattering in matter:[12,41]

$$\lambda = \frac{E}{E_p^2[\beta \ln(\gamma E) - (C/E) + (D/E^2)]}, \quad (7)$$

where λ is the IMFP (in Å), E is the electron energy (in eV), E_p is the bulk plasmon energy (in eV), as given in Table 1, and β, γ, C, and D are parameters. Satisfactory fits were made with Eqn (7) to the calculated IMFPs for energies between 50 and 2000 eV, and values of the parameters determined for each material. Equation (7) was thus a convenient analytical representation of the calculated IMFPs (e.g. for interpolation).

SURFACE and INTERFACE ANALYSIS

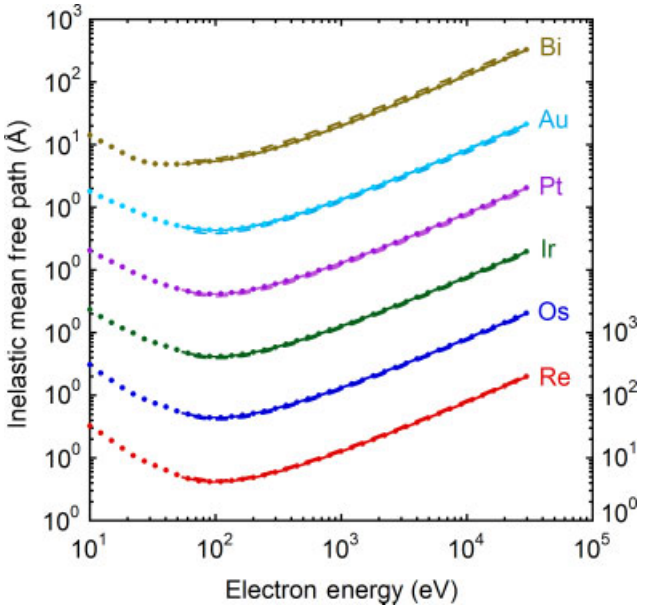

Figure 10. Plots of electron inelastic mean free paths as a function of electron energy for Re, Os, Ir, Pt, Au and Bi. See caption to Fig. 4.

The solid lines in Figs 4–10 show fits of Eqn (7) to our new set of calculated IMFPs over the 54.6–29 732.6 eV energy range. Values of β, γ, C and D from these fits are shown in Table 5 for each material. The quality of each fit was assessed from the RMS percentage difference, *RMS*:

$$RMS = 100 \times \sqrt{\sum_{i=1}^{n} \left(\frac{\lambda_{fit}(E_i) - \lambda(E_i)}{\lambda(E_i)} \right)^2 \Big/ n}, \quad (8)$$

where λ_{fit} is the IMFP obtained from the fit, λ is the calculated IMFP (each for a particular energy E_i), and $n = 64$ is the number of electron energies listed in Table 4. Values of *RMS* are also shown in Table 5 for each material. The average of the *RMS* values in Table 5 was 0.48% and the maximum value was 0.94% (for Co and Cu). These results were almost the same as those found in our previous fits of calculated IMFPs for the 50–2 000 eV energy range (average value of *RMS* = 0.40%, maximum value of *RMS* = 0.87% (for Sn)).[4,10] We again conclude that the modified Bethe equation provides a satisfactory description of the energy dependence of the calculated IMFPs in Table 4 over the 50 eV–30 keV energy range.

A useful check in our analysis is to determine values of β valid for 'high' electron energies. Such values, designated β_{opt}, represent the slopes of Fano plots (described below) in the asymptotic Bethe region and can be obtained from the following relations:[3]

$$\beta_{opt} = M_{tot}^2/28.8N_v \quad (\text{eV}^{-1}\ \text{Å}^{-1}) \quad (9a)$$

$$M_{tot}^2 = \frac{2R\int_0^{\Delta E_{max}} \text{Im}[-1/\varepsilon(\Delta E)]d(\Delta E)}{\pi\hbar^2\Omega_P^2}, \quad (9b)$$

where M_{tot}^2 is the square of the dipole matrix element for all possible inelastic-scattering processes and R is the Rydberg energy. Table 5 shows values of β_{opt} calculated from Eqn (9) where the upper limit of the integral has been chosen to be 30 keV. We see that values of β in Table 5 typically exceed those of β_{opt} by amounts varying from 0% to 10%, with an average relative difference of 4.7%. Similar results have been obtained previously and indicate that the asymptotic Bethe region may be reached only at higher energies.[10,42]

We now evaluate the validity of the modified Bethe equation [Eqn (7)] in describing the energy dependences of our calculated IMFPs using three measures of the slopes of Fano plots for five illustrative solids (Li, Si, Ni, Ag and Pt). A Fano plot (in which E/λ is plotted versus ln E) is a convenient means of testing whether a particular set of IMFP data is consistent with the original Bethe equation for inelastic scattering.[12,41,43] The slope of a Fano plot, $SLFP(E_i)$ at an energy E_i, or equivalently $SLFP(\Delta E_{max})$, would be expected from Eqns (7) and (9) to be given by,

$$SLFP(\Delta E_{max}) = E_P^2\beta_{opt}, \quad (10)$$

at sufficiently high electron energies (the so-called asymptotic Bethe limit) where the second and third terms in the denominator of Eqn (7) would be negligibly small). The dashed lines in Figs 12 and 13 show plots of $SLFP(\Delta E_{max})$ from Eqn (10) for the five selected solids as a function of ΔE_{max} where β_{opt} has been determined from Eqn (9a).

A second measure of $SLFP(E_i)$ as a function of electron energy can be obtained directly from differences of values of E/λ:

$$SLFP(E_i) = \frac{E_{i+1}/\lambda(E_{i+1}) - E_{i-1}/\lambda(E_{i-1})}{\ln(E_{i+1}/E_{i-1})} \quad (11)$$

The solid diamonds in Figs 12 and 13 show values of $SLFP(E_i)$ calculated for the same solids from Eqn (11) as a function of E_i.

A third measure of $SLFP(E_i)$ can be calculated by rearranging Eqn (7) and differentiating to yield:

$$SLFP(E_i) = \frac{d(E/\lambda)}{d\ln E} = E_P^2\left(\beta + \frac{C}{E} - \frac{2D}{E^2}\right). \quad (12)$$

The solid lines in Figs 12 and 13 show plots of $SLFP(E_i)$ for the five solids as a function of E_i from Eqn (12) using values of β, C, and D from Table 5.

We see that the plots of $SLFP(E_i)$ from Eqns (11) and (12) for each solid show similar dependences on energy although, as expected, the $SLFP(E_i)$ values from Eqn (12), a relatively simple equation, do not show the structures revealed by $SLFP(E_i)$ values from the IMFP data with Eqn (11). At our maximum values of E and ΔE_{max} (30 keV), there is satisfactory agreement of the $SLFP(\Delta E_{max})$ and $SLFP(E_i)$ values from Eqns (10) and (11), with some differences from the $SLFP(E_i)$ values from Eqn (12) for Ni and Pt that are probably associated with the limited validity of Eqn (7) in fitting the calculated IMFPs over a wide energy range.

The plots for the low-Z elements Li and Si in Fig. 12 show structure that can be associated with contributions from valence-electron excitations (bulk plasmons), K-shell excitations (Li and Si), and L-shell excitations (Si). For the medium-Z (Ni and Ag) and high-Z (Pt) elements, the plots in Figs 12 and 13 show additional structure and larger variations than for Li and Si that are due to the additional inelastic-scattering channels that are available for the former solids. We note that Eqn (12) does not provide a good representation of the *SLFP* trends for Li and Si at low energies ($E < 80$ eV) in Fig. 12. That is, Eqn (7) is generally satisfactory for fitting the calculated IMFPs for energies down to 50 eV (cf. Figures 4 and 5) but does not adequately describe the energy dependences

Table 4. Calculated IMFPs for the 41 elemental solids as a function of electron kinetic energy *E*

	Inelastic mean free path (Å)						
E (eV)	Li	Be	C (Graphite)	C (Diamond)	C (Glassy)	Na	Mg
54.6	4.84	3.56	4.57	6.25	5.75	5.25	4.10
60.3	5.12	3.60	4.40	5.69	5.77	5.56	4.26
66.7	5.43	3.68	4.30	5.26	5.77	5.90	4.45
73.7	5.77	3.78	4.27	4.96	5.84	6.27	4.66
81.5	6.14	3.91	4.29	4.77	5.96	6.66	4.89
90.0	6.54	4.07	4.35	4.68	6.12	7.08	5.15
99.5	6.98	4.25	4.44	4.65	6.30	7.53	5.42
109.9	7.45	4.45	4.57	4.68	6.54	8.01	5.72
121.5	7.97	4.68	4.73	4.76	6.80	8.53	6.06
134.3	8.53	4.94	4.92	4.88	7.11	9.09	6.41
148.4	9.15	5.22	5.14	5.04	7.44	9.70	6.80
164.0	9.81	5.53	5.39	5.23	7.83	10.4	7.22
181.3	10.5	5.87	5.67	5.46	8.26	11.1	7.67
200.3	11.3	6.24	5.99	5.71	8.81	11.8	8.16
221.4	12.1	6.65	6.33	6.00	9.34	12.7	8.69
244.7	13.1	7.09	6.72	6.33	9.86	13.6	9.27
270.4	14.1	7.58	7.14	6.70	10.5	14.6	9.90
298.9	15.1	8.11	7.61	7.10	11.2	15.7	10.6
330.3	16.4	8.76	8.12	7.52	12.0	17.0	11.4
365.0	17.7	9.38	8.69	8.02	12.8	18.3	12.2
403.4	19.2	10.1	9.31	8.56	13.8	19.7	13.1
445.9	20.7	10.8	9.99	9.16	14.8	21.2	14.0
492.7	22.4	11.6	10.7	9.81	15.9	22.9	15.1
544.6	24.3	12.5	11.5	10.5	17.1	24.7	16.2
601.8	26.3	13.5	12.4	11.3	18.4	26.7	17.5
665.1	28.5	14.5	13.4	12.1	19.8	28.9	18.9
735.1	30.9	15.7	14.4	13.0	21.4	31.3	20.4
812.4	33.5	16.9	15.5	14.0	23.0	33.8	22.0
897.8	36.4	18.3	16.8	15.1	24.8	36.7	23.8
992.3	39.5	19.8	18.1	16.3	26.8	39.8	25.7
1096.6	42.9	21.4	19.6	17.6	29.0	43.1	27.8
1212.0	46.6	23.2	21.1	19.0	31.4	46.8	30.2
1339.4	50.7	25.1	22.9	20.5	33.9	50.9	32.7
1480.3	55.1	27.3	24.8	22.1	36.7	55.2	35.4
1636.0	59.9	29.6	26.8	24.0	39.8	60.0	38.4
1808.0	65.2	32.1	29.1	25.9	43.1	65.3	41.7
1998.2	71.0	34.8	31.5	28.1	46.8	71.0	45.3
2208.3	77.3	37.8	34.2	30.4	50.8	77.2	49.2
2440.6	84.2	41.1	37.1	33.0	55.1	84.0	53.5
2697.3	91.7	44.7	40.3	35.8	59.9	91.4	58.1
2981.0	99.9	48.6	43.8	38.8	65.0	99.6	63.2
3294.5	108.9	52.8	47.6	42.1	70.7	108.4	68.7
3640.9	118.7	57.5	51.7	45.8	76.9	118.1	74.8
4023.9	129.4	62.6	56.3	49.7	83.6	128.6	81.4
4447.1	141.1	68.1	61.2	54.0	90.9	140.2	88.6
4914.8	153.9	74.2	66.6	58.8	99.0	152.8	96.4
5431.7	167.9	80.8	72.5	63.9	107.7	166.6	105.0
6002.9	183.2	88.0	78.9	69.5	117.3	181.6	114.4
6634.2	199.9	95.9	85.9	75.6	127.8	198.1	124.7
7332.0	218.2	104.5	93.6	82.3	139.2	216.1	135.9
8103.1	238.2	113.9	102.0	89.6	151.7	235.8	148.1
8955.3	260.1	124.2	111.1	97.6	165.3	257.3	161.5
9897.1	284.0	135.5	121.1	106.3	180.2	280.8	176.1
10938.0	310.2	147.8	132.0	115.9	196.5	306.5	192.1
12088.4	338.8	161.2	144.0	126.3	214.3	334.7	209.6
13359.7	370.1	175.9	157.0	137.6	233.8	365.4	228.7

Table 4. (*continued*)

	Inelastic mean free path (Å)						
E (eV)	Li	Be	C (Graphite)	C (Diamond)	C (Glassy)	Na	Mg
14764.8	404.4	192.0	171.3	150.1	255.1	399.1	249.6
16317.6	441.9	209.6	186.9	163.6	278.4	435.9	272.4
18033.7	483.0	228.8	204.0	178.5	303.8	476.3	297.4
19930.4	527.9	249.8	222.6	194.7	331.6	520.3	324.7
22026.5	577.1	272.8	243.0	212.4	362.1	568.6	354.6
24343.0	631.0	298.0	265.3	231.8	395.4	621.4	387.3
26903.2	689.9	325.5	289.7	253.0	431.8	679.2	423.0
29732.6	754.5	355.6	316.4	276.2	471.6	742.5	462.2

	Inelastic mean free path (Å)						
E (eV)	Al	Si	K	Sc	Ti	V	Cr
54.6	3.58	4.18	7.39	4.58	4.11	4.54	4.34
60.3	3.68	4.29	7.72	4.57	4.09	4.49	4.26
66.7	3.82	4.42	8.08	4.57	4.09	4.48	4.21
73.7	3.97	4.59	8.48	4.60	4.12	4.49	4.21
81.5	4.15	4.78	8.95	4.67	4.19	4.54	4.24
90.0	4.34	5.00	9.42	4.76	4.28	4.62	4.30
99.5	4.56	5.25	9.93	4.88	4.40	4.71	4.40
109.9	4.81	5.52	10.5	5.00	4.51	4.82	4.51
121.5	5.08	5.82	11.2	5.15	4.64	4.97	4.66
134.3	5.37	6.16	11.9	5.33	4.79	5.12	4.82
148.4	5.69	6.52	12.7	5.56	4.98	5.30	5.01
164.0	6.03	6.92	13.6	5.84	5.21	5.50	5.21
181.3	6.41	7.35	14.6	6.15	5.47	5.73	5.44
200.3	6.82	7.81	15.6	6.50	5.77	5.99	5.70
221.4	7.28	8.32	16.8	6.89	6.10	6.29	6.00
244.7	7.75	8.88	18.1	7.32	6.47	6.63	6.32
270.4	8.28	9.49	19.4	7.80	6.88	7.01	6.69
298.9	8.84	10.2	21.0	8.33	7.32	7.42	7.09
330.3	9.56	11.0	22.8	8.91	7.82	7.86	7.53
365.0	10.2	11.8	24.6	9.55	8.36	8.37	8.02
403.4	10.9	12.6	26.6	10.2	8.95	8.93	8.55
445.9	11.7	13.5	28.7	11.0	9.60	9.54	9.13
492.7	12.6	14.5	31.1	11.8	10.3	10.2	9.77
544.6	13.5	15.5	33.6	12.7	11.1	10.9	10.5
601.8	14.5	16.7	36.4	13.7	11.9	11.7	11.2
665.1	15.6	18.0	39.5	14.8	12.8	12.6	12.1
735.1	16.9	19.4	42.8	15.9	13.9	13.6	13.0
812.4	18.2	20.9	46.3	17.2	14.9	14.6	14.0
897.8	19.6	22.5	50.2	18.6	16.1	15.8	15.0
992.3	21.2	24.3	54.5	20.1	17.4	17.0	16.2
1096.6	22.9	26.3	59.1	21.8	18.9	18.4	17.5
1212.0	24.8	28.5	64.1	23.5	20.4	19.8	18.9
1339.4	26.9	30.8	69.6	25.5	22.1	21.4	20.5
1480.3	29.1	33.4	75.6	27.6	23.9	23.2	22.1
1636.0	31.6	36.2	82.1	29.9	25.8	25.1	23.9
1808.0	34.2	39.2	89.2	32.4	28.0	27.1	25.9
1998.2	37.1	42.5	97.0	35.1	30.3	29.4	28.0
2208.3	40.3	46.2	105.5	38.1	32.9	31.8	30.3
2440.6	43.8	50.1	114.8	41.3	35.7	34.5	32.9
2697.3	47.6	54.5	125.0	44.9	38.7	37.4	35.6
2981.0	51.7	59.2	136.0	48.7	42.0	40.5	38.6
3294.5	56.2	64.3	148.1	53.0	45.7	44.0	41.9
3640.9	61.1	70.0	161.4	57.6	49.6	47.7	45.5
4023.9	66.5	76.1	175.8	62.6	53.9	51.9	49.4

Table 4. (*continued*)

	Inelastic mean free path (Å)						
E (eV)	Al	Si	K	Sc	Ti	V	Cr
4447.1	72.4	82.8	191.6	68.1	58.6	56.3	53.7
4914.8	78.8	90.1	208.8	74.1	63.8	61.2	58.4
5431.7	85.8	98.1	227.7	80.6	69.4	66.6	63.5
6002.9	93.4	106.9	248.3	87.8	75.5	72.4	69.0
6634.2	101.7	116.4	270.8	95.6	82.2	78.8	75.1
7332.0	110.8	126.8	295.4	104.1	89.5	85.7	81.7
8103.1	120.8	138.2	322.4	113.4	97.5	93.3	88.9
8955.3	131.7	150.6	351.8	123.6	106.2	101.6	96.8
9897.1	143.6	164.2	384.0	134.7	115.7	110.7	105.4
10938.0	156.5	179.1	419.2	146.8	126.1	120.6	114.9
12088.4	170.7	195.3	457.7	160.1	137.5	131.4	125.2
13359.7	186.3	213.0	499.8	174.6	149.9	143.2	136.4
14764.8	203.2	232.4	545.9	190.4	163.5	156.1	148.7
16317.6	221.8	253.6	596.3	207.8	178.3	170.2	162.1
18033.7	242.1	276.8	651.4	226.7	194.6	185.6	176.8
19930.4	264.2	302.2	711.8	247.4	212.3	202.5	192.8
22026.5	288.5	329.9	777.8	270.1	231.7	220.9	210.4
24343.0	315.1	360.3	850.1	294.8	252.9	241.0	229.5
26903.2	344.1	393.5	929.2	321.9	276.1	263.0	250.5
29732.6	375.9	429.8	1015.8	351.5	301.5	287.1	273.4

	Inelastic mean free path (Å)					
E (eV)	Fe	Co	Ni	Cu	Ge	Y
54.6	4.28	4.84	4.77	4.94	4.08	5.04
60.3	4.25	4.68	4.68	4.87	4.18	5.05
66.7	4.26	4.58	4.59	4.84	4.31	5.09
73.7	4.30	4.52	4.58	4.84	4.45	5.16
81.5	4.37	4.51	4.55	4.87	4.62	5.25
90.0	4.47	4.52	4.59	4.93	4.80	5.36
99.5	4.57	4.55	4.63	5.00	5.02	5.50
109.9	4.70	4.61	4.70	5.11	5.25	5.67
121.5	4.86	4.70	4.80	5.24	5.51	5.89
134.3	5.05	4.83	4.92	5.40	5.79	6.15
148.4	5.25	4.98	5.07	5.58	6.09	6.46
164.0	5.47	5.13	5.24	5.79	6.43	6.81
181.3	5.71	5.30	5.45	6.02	6.79	7.20
200.3	5.98	5.50	5.67	6.29	7.18	7.64
221.4	6.28	5.74	5.91	6.58	7.61	8.13
244.7	6.61	6.00	6.19	6.90	8.07	8.66
270.4	6.97	6.30	6.49	7.25	8.58	9.24
298.9	7.38	6.63	6.83	7.64	9.13	9.88
330.3	7.85	7.00	7.23	8.15	9.86	10.7
365.0	8.33	7.41	7.64	8.60	10.5	11.5
403.4	8.86	7.85	8.09	9.11	11.2	12.3
445.9	9.44	8.35	8.60	9.67	12.0	13.2
492.7	10.1	8.89	9.15	10.3	12.8	14.2
544.6	10.8	9.49	9.75	10.9	13.7	15.3
601.8	11.5	10.1	10.4	11.7	14.7	16.4
665.1	12.4	10.9	11.1	12.5	15.8	17.7
735.1	13.3	11.6	11.9	13.4	16.9	19.1
812.4	14.3	12.5	12.8	14.3	18.2	20.6
897.8	15.4	13.4	13.8	15.4	19.6	22.2
992.3	16.6	14.5	14.8	16.6	21.1	23.9
1096.6	17.9	15.6	15.9	17.8	22.8	25.8
1212.0	19.3	16.8	17.2	19.2	24.6	27.9

Table 4. (*continued*)

	Inelastic mean free path (Å)					
E (eV)	Fe	Co	Ni	Cu	Ge	Y
1339.4	20.8	18.1	18.5	20.7	26.6	30.2
1480.3	22.5	19.6	20.0	22.3	28.7	32.7
1636.0	24.3	21.1	21.6	24.1	31.1	35.3
1808.0	26.3	22.9	23.4	26.1	33.6	38.3
1998.2	28.5	24.7	25.3	28.2	36.4	41.5
2208.3	30.9	26.8	27.4	30.5	39.5	45.0
2440.6	33.4	29.0	29.7	33.1	42.8	48.8
2697.3	36.2	31.4	32.1	35.8	46.5	53.0
2981.0	39.3	34.0	34.8	38.8	50.4	57.5
3294.5	42.6	36.9	37.7	42.1	54.8	62.5
3640.9	46.3	40.0	40.9	45.6	59.5	67.9
4023.9	50.2	43.4	44.4	49.5	64.7	73.8
4447.1	54.5	47.1	48.2	53.7	70.3	80.3
4914.8	59.3	51.2	52.3	58.3	76.4	87.3
5431.7	64.4	55.6	56.9	63.4	83.1	95.0
6002.9	70.0	60.4	61.8	68.8	90.4	103.4
6634.2	76.2	65.7	67.2	74.8	98.4	112.6
7332.0	82.9	71.5	73.1	81.4	107.1	122.6
8103.1	90.2	77.7	79.5	88.5	116.6	133.5
8955.3	98.2	84.6	86.5	96.3	127.0	145.5
9897.1	106.9	92.1	94.1	104.8	138.3	158.5
10938.0	116.4	100.3	102.5	114.1	150.7	172.8
12088.4	126.8	109.2	111.6	124.3	164.2	188.3
13359.7	138.2	118.9	121.6	135.4	179.0	205.3
14764.8	150.6	129.6	132.4	147.5	195.2	223.9
16317.6	164.2	141.2	144.3	160.7	212.9	244.3
18033.7	179.0	153.9	157.3	175.2	232.2	266.5
19930.4	195.2	167.8	171.5	191.0	253.4	290.8
22026.5	212.9	183.0	187.0	208.2	276.5	317.4
24343.0	232.3	199.6	204.0	227.1	301.8	346.4
26903.2	253.5	217.8	222.5	247.7	329.4	378.2
29732.6	276.7	237.6	242.8	270.3	359.6	413.0

	Inelastic mean free path (Å)						
E (eV)	Nb	Mo	Ru	Rh	Pd	Ag	In
54.6	5.50	4.77	4.68	4.57	4.64	5.91	4.79
60.3	5.36	4.56	4.46	4.37	4.44	5.63	4.86
66.7	5.26	4.44	4.29	4.21	4.27	5.39	4.95
73.7	5.21	4.37	4.16	4.08	4.16	5.18	5.05
81.5	5.20	4.34	4.09	4.01	4.08	5.05	5.16
90.0	5.24	4.35	4.05	3.96	4.04	4.94	5.28
99.5	5.30	4.39	4.05	3.96	4.04	4.88	5.43
109.9	5.38	4.47	4.09	3.99	4.07	4.87	5.59
121.5	5.47	4.56	4.15	4.05	4.13	4.89	5.78
134.3	5.59	4.66	4.25	4.14	4.21	4.94	6.00
148.4	5.75	4.79	4.37	4.25	4.33	5.01	6.24
164.0	5.95	4.96	4.51	4.39	4.47	5.13	6.51
181.3	6.20	5.16	4.67	4.54	4.63	5.28	6.81
200.3	6.49	5.40	4.86	4.72	4.81	5.46	7.15
221.4	6.82	5.68	5.08	4.92	5.02	5.66	7.52
244.7	7.20	5.99	5.34	5.16	5.26	5.89	7.93
270.4	7.62	6.34	5.63	5.43	5.53	6.16	8.37
298.9	8.09	6.72	5.96	5.73	5.85	6.47	8.87
330.3	8.62	7.15	6.30	6.04	6.16	6.74	9.34
365.0	9.21	7.63	6.71	6.43	6.56	7.15	9.96
403.4	9.85	8.16	7.16	6.85	7.00	7.61	10.6

Table 4. (*continued*)

	Inelastic mean free path (Å)						
E (eV)	Nb	Mo	Ru	Rh	Pd	Ag	In
445.9	10.6	8.74	7.66	7.32	7.48	8.11	11.4
492.7	11.3	9.37	8.20	7.84	8.01	8.66	12.2
544.6	12.1	10.1	8.79	8.40	8.58	9.26	13.1
601.8	13.0	10.8	9.44	9.01	9.21	9.92	14.1
665.1	14.0	11.6	10.1	9.68	9.90	10.6	15.1
735.1	15.0	12.5	10.9	10.4	10.6	11.4	16.3
812.4	16.1	13.4	11.7	11.2	11.5	12.3	17.6
897.8	17.4	14.4	12.6	12.1	12.3	13.2	18.9
992.3	18.7	15.5	13.6	13.0	13.3	14.2	20.4
1096.6	20.1	16.7	14.6	14.0	14.3	15.2	22.1
1212.0	21.7	18.0	15.8	15.1	15.4	16.4	23.9
1339.4	23.4	19.4	17.0	16.2	16.7	17.7	25.8
1480.3	25.3	21.0	18.3	17.5	18.0	19.0	27.9
1636.0	27.3	22.6	19.8	18.9	19.4	20.5	30.1
1808.0	29.5	24.5	21.4	20.4	21.0	22.2	32.6
1998.2	31.9	26.4	23.1	22.1	22.7	23.9	35.3
2208.3	34.5	28.6	25.0	23.9	24.5	25.9	38.2
2440.6	37.4	31.0	27.1	25.8	26.6	28.0	41.4
2697.3	40.5	33.6	29.3	28.0	28.8	30.3	44.9
2981.0	43.9	36.4	31.8	30.3	31.2	32.8	48.6
3294.5	47.6	39.5	34.4	32.9	33.8	35.6	52.8
3640.9	51.7	42.8	37.3	35.6	36.7	38.6	57.3
4023.9	56.1	46.5	40.5	38.7	39.8	41.8	62.2
4447.1	60.9	50.5	44.0	42.0	43.2	45.4	67.6
4914.8	66.2	54.8	47.8	45.6	46.9	49.3	73.4
5431.7	71.9	59.6	51.9	49.5	51.0	53.6	79.8
6002.9	78.2	64.8	56.4	53.8	55.4	58.2	86.8
6634.2	85.1	70.4	61.3	58.5	60.2	63.2	94.4
7332.0	92.5	76.6	66.7	63.6	65.5	68.8	102.7
8103.1	100.7	83.4	72.6	69.2	71.3	74.8	111.8
8955.3	109.6	90.7	79.0	75.3	77.5	81.4	121.8
9897.1	119.3	98.8	86.0	82.0	84.4	88.5	132.6
10938.0	129.9	107.5	93.6	89.3	91.9	96.4	144.4
12088.4	141.5	117.1	101.9	97.2	100.1	104.9	157.4
13359.7	154.2	127.6	111.0	105.9	109.0	114.3	171.5
14764.8	168.0	139.1	121.0	115.4	118.8	124.5	186.9
16317.6	183.1	151.6	131.8	125.8	129.5	135.6	203.8
18033.7	199.6	165.2	143.7	137.1	141.1	147.8	222.2
19930.4	217.7	180.2	156.7	149.4	153.9	161.1	242.4
22026.5	237.4	196.5	170.8	162.9	167.8	175.7	264.4
24343.0	259.0	214.3	186.3	177.7	183.0	191.6	288.5
26903.2	282.5	233.8	203.3	193.9	199.6	208.9	314.8
29732.6	308.3	255.1	221.8	211.5	217.8	227.9	343.6

	Inelastic mean free path (Å)						
E (eV)	Sn	Cs	Gd	Tb	Dy	Hf	Ta
54.6	5.82	6.57	4.14	4.08	4.44	5.43	4.71
60.3	5.88	6.92	4.15	4.06	4.39	5.37	4.58
66.7	5.94	7.31	4.19	4.06	4.37	5.33	4.51
73.7	6.03	7.74	4.26	4.09	4.40	5.33	4.47
81.5	6.12	8.22	4.36	4.14	4.44	5.34	4.48
90.0	6.26	8.73	4.48	4.21	4.50	5.39	4.49
99.5	6.39	9.29	4.61	4.29	4.59	5.46	4.54
109.9	6.57	9.89	4.79	4.40	4.70	5.55	4.60
121.5	6.78	10.5	5.01	4.54	4.84	5.67	4.70

Table 4. (*continued*)

E (eV)	Inelastic mean free path (Å)						
	Sn	Cs	Gd	Tb	Dy	Hf	Ta
134.3	7.01	11.3	5.25	4.71	5.01	5.81	4.82
148.4	7.27	12.0	5.51	4.92	5.22	5.98	4.95
164.0	7.55	12.9	5.79	5.15	5.44	6.19	5.11
181.3	7.87	13.8	6.11	5.40	5.71	6.43	5.30
200.3	8.22	14.8	6.46	5.70	6.01	6.72	5.52
221.4	8.62	15.9	6.86	6.02	6.34	7.03	5.77
244.7	9.05	17.1	7.28	6.38	6.70	7.39	6.05
270.4	9.53	18.4	7.74	6.78	7.11	7.79	6.37
298.9	10.1	19.8	8.24	7.21	7.55	8.23	6.72
330.3	10.5	21.4	8.93	7.76	8.13	8.80	7.17
365.0	11.2	23.0	9.51	8.27	8.65	9.34	7.60
403.4	11.9	24.8	10.2	8.83	9.22	9.92	8.07
445.9	12.8	26.8	10.9	9.44	9.84	10.6	8.58
492.7	13.6	28.9	11.6	10.1	10.5	11.2	9.14
544.6	14.6	31.3	12.5	10.8	11.3	12.0	9.74
601.8	15.7	33.8	13.4	11.6	12.1	12.8	10.4
665.1	16.8	36.6	14.4	12.5	13.0	13.7	11.1
735.1	18.1	39.7	15.5	13.5	13.9	14.7	11.9
812.4	19.5	43.0	16.7	14.5	15.0	15.7	12.8
897.8	21.0	46.6	18.0	15.6	16.2	16.9	13.7
992.3	22.6	50.5	19.4	16.8	17.4	18.1	14.7
1096.6	24.4	54.8	21.0	18.2	18.8	19.5	15.8
1212.0	26.4	59.5	22.7	19.6	20.3	21.0	17.0
1339.4	28.5	64.6	24.5	21.2	21.9	22.6	18.3
1480.3	30.8	70.2	26.5	23.0	23.7	24.4	19.7
1636.0	33.3	76.3	28.7	24.8	25.6	26.3	21.3
1808.0	36.0	82.9	31.1	26.9	27.7	28.4	23.0
1998.2	38.9	90.1	33.7	29.1	30.0	30.7	24.8
2208.3	42.1	98.0	36.5	31.6	32.5	33.2	26.8
2440.6	45.6	106.6	39.6	34.3	35.2	35.9	29.0
2697.3	49.4	115.9	43.0	37.2	38.2	38.9	31.4
2981.0	53.5	126.2	46.6	40.3	41.5	42.1	34.0
3294.5	58.0	137.3	50.7	43.8	45.0	45.6	36.8
3640.9	63.0	149.5	55.0	47.6	48.9	49.5	39.9
4023.9	68.3	162.8	59.8	51.7	53.1	53.7	43.3
4447.1	74.2	177.3	65.0	56.2	57.6	58.3	47.0
4914.8	80.6	193.2	70.6	61.1	62.6	63.3	51.0
5431.7	87.6	210.6	76.8	66.4	68.1	68.7	55.4
6002.9	95.2	229.5	83.5	72.2	74.0	74.6	60.2
6634.2	103.5	250.3	90.9	78.6	80.5	81.1	65.4
7332.0	112.6	272.9	98.9	85.5	87.6	88.1	71.0
8103.1	122.6	297.7	107.6	93.1	95.4	95.8	77.2
8955.3	133.4	324.8	117.2	101.3	103.8	104.2	84.0
9897.1	145.2	354.4	127.7	110.4	113.0	113.4	91.4
10938.0	158.1	386.8	139.1	120.2	123.1	123.4	99.4
12088.4	172.3	422.2	151.6	131.0	134.1	134.3	108.2
13359.7	187.7	460.9	165.2	142.8	146.2	146.3	117.8
14764.8	204.5	503.3	180.1	155.7	159.3	159.3	128.3
16317.6	222.9	549.7	196.4	169.7	173.7	173.6	139.8
18033.7	243.0	600.4	214.2	185.1	189.4	189.1	152.3
19930.4	265.0	655.9	233.7	201.9	206.6	206.1	166.0
22026.5	289.0	716.6	255.0	220.3	225.3	224.7	180.9
24343.0	315.2	783.0	278.2	240.4	245.8	245.0	197.2
26903.2	343.9	855.8	303.7	262.4	268.2	267.2	215.1
29732.6	375.3	935.3	331.5	286.4	292.8	291.5	234.6

Table 4. (*continued*)

	Inelastic mean free path (Å)						
E (eV)	W	Re	Os	Ir	Pt	Au	Bi
54.6	5.04	5.04	5.29	5.01	4.81	4.95	4.96
60.3	4.77	4.73	5.01	4.74	4.59	4.75	5.02
66.7	4.60	4.49	4.77	4.53	4.44	4.60	5.09
73.7	4.49	4.32	4.61	4.36	4.30	4.49	5.15
81.5	4.43	4.22	4.50	4.25	4.21	4.41	5.27
90.0	4.41	4.18	4.43	4.19	4.16	4.38	5.40
99.5	4.43	4.17	4.41	4.16	4.15	4.34	5.54
109.9	4.49	4.20	4.44	4.18	4.19	4.36	5.70
121.5	4.57	4.25	4.51	4.23	4.25	4.40	5.88
134.3	4.67	4.33	4.59	4.31	4.34	4.48	6.09
148.4	4.78	4.44	4.69	4.41	4.45	4.58	6.31
164.0	4.92	4.57	4.82	4.55	4.59	4.72	6.57
181.3	5.09	4.71	4.97	4.70	4.75	4.88	6.86
200.3	5.28	4.89	5.14	4.87	4.95	5.07	7.17
221.4	5.51	5.09	5.35	5.07	5.17	5.29	7.53
244.7	5.77	5.32	5.59	5.31	5.41	5.54	7.93
270.4	6.06	5.59	5.86	5.57	5.68	5.82	8.36
298.9	6.38	5.89	6.16	5.86	5.99	6.13	8.85
330.3	6.79	6.25	6.55	6.22	6.36	6.47	9.35
365.0	7.19	6.62	6.93	6.60	6.74	6.87	9.96
403.4	7.63	7.03	7.34	7.00	7.16	7.31	10.6
445.9	8.11	7.47	7.80	7.45	7.62	7.78	11.4
492.7	8.62	7.94	8.29	7.93	8.12	8.29	12.2
544.6	9.19	8.47	8.83	8.45	8.66	8.87	13.0
601.8	9.80	9.03	9.42	9.02	9.24	9.47	14.0
665.1	10.5	9.65	10.1	9.63	9.88	10.1	15.0
735.1	11.2	10.3	10.7	10.3	10.6	10.8	16.1
812.4	12.0	11.1	11.5	11.0	11.3	11.6	17.3
897.8	12.8	11.8	12.3	11.8	12.1	12.5	18.7
992.3	13.8	12.7	13.2	12.7	13.0	13.4	20.1
1096.6	14.8	13.6	14.2	13.6	14.0	14.4	21.7
1212.0	15.9	14.7	15.2	14.6	15.0	15.5	23.3
1339.4	17.1	15.8	16.4	15.7	16.2	16.7	25.2
1480.3	18.4	17.0	17.6	16.9	17.4	18.0	27.2
1636.0	19.9	18.3	19.0	18.2	18.8	19.4	29.4
1808.0	21.4	19.8	20.5	19.7	20.3	21.0	31.8
1998.2	23.1	21.3	22.1	21.2	21.9	22.6	34.3
2208.3	25.0	23.0	23.8	22.9	23.6	24.5	37.2
2440.6	27.0	24.9	25.8	24.8	25.5	26.5	40.2
2697.3	29.2	26.9	27.8	26.8	27.6	28.6	43.6
2981.0	31.6	29.2	30.1	29.0	29.9	31.0	47.2
3294.5	34.3	31.6	32.6	31.4	32.4	33.6	51.2
3640.9	37.1	34.2	35.3	34.0	35.1	36.4	55.6
4023.9	40.3	37.1	38.3	36.8	38.0	39.5	60.3
4447.1	43.7	40.2	41.5	39.9	41.2	42.8	65.5
4914.8	47.4	43.6	45.0	43.3	44.7	46.4	71.1
5431.7	51.4	47.4	48.9	47.0	48.6	50.4	77.3
6002.9	55.9	51.5	53.1	51.1	52.7	54.8	84.0
6634.2	60.7	55.9	57.6	55.5	57.3	59.5	91.4
7332.0	65.9	60.7	62.6	60.3	62.2	64.7	99.4
8103.1	71.6	66.0	68.0	65.5	67.6	70.3	108.1
8955.3	77.9	71.8	74.0	71.2	73.6	76.5	117.7
9897.1	84.7	78.0	80.4	77.4	80.0	83.2	128.1
10938.0	92.2	84.9	87.5	84.2	87.0	90.5	139.5
12088.4	100.3	92.4	95.2	91.6	94.7	98.5	152.0
13359.7	109.2	100.6	103.6	99.7	103.1	107.3	165.5

Table 4. (*continued*)

	Inelastic mean free path (Å)						
E (eV)	W	Re	Os	Ir	Pt	Au	Bi
14764.8	118.9	109.5	112.8	108.6	112.2	116.8	180.4
16317.6	129.5	119.2	122.8	118.3	122.2	127.2	196.6
18033.7	141.0	129.9	133.7	128.8	133.2	138.6	214.3
19930.4	153.7	141.5	145.7	140.3	145.1	151.0	233.7
22026.5	167.5	154.2	158.8	152.9	158.1	164.6	254.9
24343.0	182.6	168.1	173.1	166.7	172.4	179.5	278.0
26903.2	199.1	183.3	188.7	181.8	187.9	195.7	303.3
29732.6	217.1	199.9	205.7	198.2	205.0	213.4	331.0

Table 5. Values of the parameters β, γ, C, and D found in the fits of Eqn (7) to the calculated IMFPs for each elemental solid, values of β_{opt} calculated from Eqn (9), and values of *RMS* calculated from Eqn (8)

Element	β_{opt} (eV^{-1} Å^{-1})	β (eV^{-1} Å^{-1})	γ (eV^{-1})	C (Å^{-1})	D (eV Å^{-1})	*RMS* (%)
Li	0.0646	0.0653	0.4340	3.091	81.4	0.16
Be	0.0279	0.0290	0.1668	1.591	31.2	0.35
C (graphite)	0.0177	0.0183	0.1333	1.365	23.6	0.20
C (diamond)	0.0135	0.0139	0.1022	1.271	24.9	0.27
C (glassy)	0.0147	0.0153	0.1380	1.072	23.3	0.28
Na	0.1236	0.1258	0.3030	7.846	268.1	0.24
Mg	0.0618	0.0642	0.1648	3.801	126.5	0.49
Al	0.0367	0.0389	0.1258	1.629	50.3	0.61
Si	0.0291	0.0311	0.1186	1.104	30.3	0.63
K	0.1726	0.1759	0.3041	5.119	2.1	0.33
Sc	0.0604	0.0603	0.1587	5.393	119.5	0.42
Ti	0.0378	0.0380	0.1352	3.436	88.3	0.33
V	0.0256	0.0263	0.0942	2.361	73.5	0.51
Cr	0.0196	0.0204	0.0860	1.492	43.0	0.45
Fe	0.0142	0.0151	0.0715	0.981	33.7	0.72
Co	0.0140	0.0149	0.0623	1.186	40.9	0.94
Ni	0.0123	0.0132	0.0587	0.965	34.6	0.92
Cu	0.0108	0.0117	0.0535	0.680	25.8	0.94
Ge	0.0409	0.0444	0.0781	1.592	61.4	0.74
Y	0.0685	0.0708	0.1161	3.261	43.1	0.63
Nb	0.0315	0.0324	0.0811	2.494	69.8	0.60
Mo	0.0274	0.0283	0.0771	2.000	52.0	0.53
Ru	0.0208	0.0214	0.0743	1.740	48.4	0.42
Rh	0.0198	0.0204	0.0732	1.760	51.8	0.42
Pd	0.0184	0.0188	0.0787	1.733	50.5	0.44
Ag	0.0188	0.0196	0.0628	1.933	65.0	0.65
In	0.0672	0.0693	0.0911	5.607	191.8	0.47
Sn	0.0485	0.0505	0.0752	4.016	145.9	0.73
Cs	0.2960	0.3045	0.2512	9.227	247.1	0.16
Gd	0.0279	0.0292	0.0909	1.199	26.9	0.35
Tb	0.0327	0.0337	0.0979	2.236	56.6	0.26
Dy	0.0311	0.0323	0.0846	2.049	55.8	0.29
Hf	0.0529	0.0566	0.0523	3.038	111.4	0.45
Ta	0.0428	0.0460	0.0488	2.378	87.4	0.54
W	0.0342	0.0372	0.0417	1.543	55.6	0.65
Re	0.0296	0.0321	0.0428	1.502	50.6	0.54
Os	0.0241	0.0262	0.0395	1.160	42.6	0.54
Ir	0.0223	0.0241	0.0422	1.132	38.9	0.42
Pt	0.0207	0.0223	0.0444	1.046	35.4	0.38
Au	0.0202	0.0213	0.0524	1.424	48.1	0.31
Bi	0.0576	0.0609	0.0700	3.998	146.3	0.49

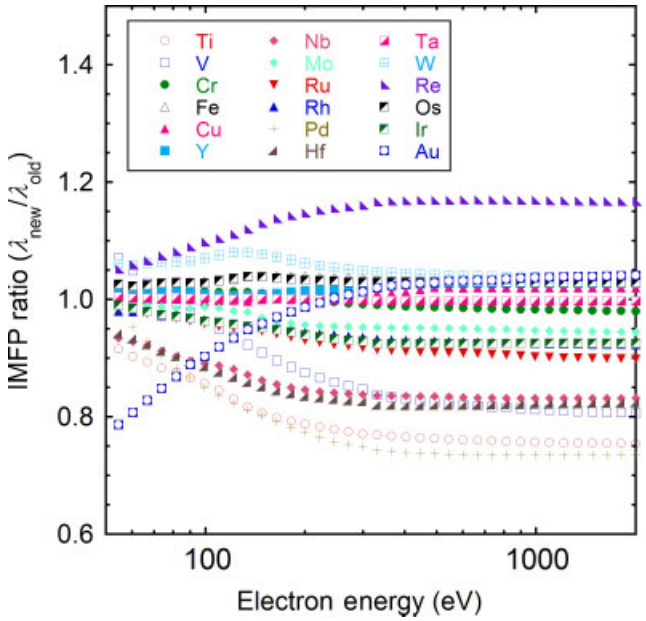

Figure 11. Plots of the ratio of the IMFPs in Table 4 for Ti, V, Cr, Fe, Cu Y, Nb, Mo, Ru, Rh, Pd, Hf, Ta, W, Re, Os, Ir and Au with the newer ELFs that we used (λ_{new}) to the corresponding IMFPs that we published previously (λ_{old}) in Ref. [4].

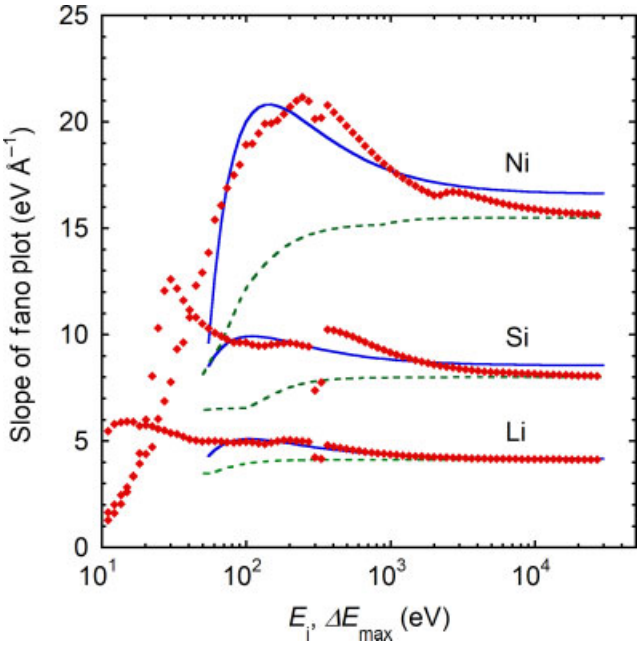

Figure 12. Plots of slopes of Fano plots for Li, Ni and Si from Eqns (10)–(12) as a function of the upper energy limit, ΔE_{max}, used in the evaluation of $E_P^2\beta_{opt}$ from Eqn (9) or of electron energy E_i. The dashed lines indicate values of the slopes calculated from Eqn (10). The solid diamonds indicate slopes calculated from the optical IMFPs (Table 4) using Eqn (11). The solid lines show slopes calculated from Eqn (12) with parameter values from Table 5 for each elemental solid. The discontinuities in the vicinity of 300 eV are artifacts associated with use of the FPA for energies between 10 eV and 300 eV and the SPA for energies between 330 eV and 30 keV.

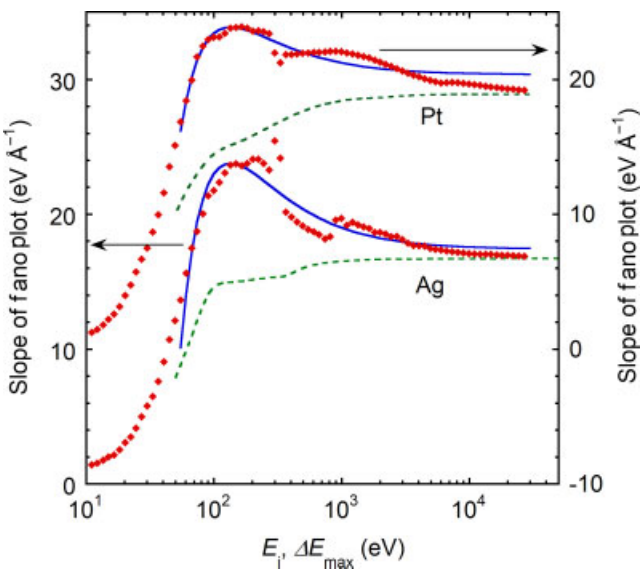

Figure 13. Plots of slopes of Fano plots for Ag and Pt. See caption to Fig. 12.

for Li and Si at such low energies. Equation (12) provides a generally good description of the *SLFP* energy dependence for Ni, Ag and Pt over the 50 eV–30 keV range.

Figures 12 and 13 also illustrate how the second and third terms in the denominator of Eqn (7) are needed to fit the calculated IMFPs over the 50 eV–30 keV energy range. For $E > 10$ keV, however, these terms are negligible and the IMFP energy dependence can be described satisfactorily by the simple Bethe equation (i.e. Equation (7) with $C = D = 0$). It is thus reasonable for the modified Bethe equation [Eqn (7)] to be useful not only for energy range for which it was originally applied (50 eV–2 keV) but also for higher energies (i.e. up to 30 keV as shown here).

We previously analyzed IMFPs for a group of 27 elemental solids[4] and a group of 14 organic compounds[7] that had been calculated from optical data for electron energies between 50 eV and 2 000 eV. Simple expressions were found for the four parameters in Eqn (7) in terms of material properties:[7]

$$\beta = -0.10 + 0.944/(E_P^2 + E_g^2)^{0.5} + 0.069\rho^{0.1} \quad (13a)$$

$$\gamma = 0.191\rho^{-0.5} \quad (13b)$$

$$C = 1.97 - 0.91U \quad (13c)$$

$$D = 53.4 - 20.8U \quad (13d)$$

$$U = N_v\rho/M = E_P^2/829.4 \quad (13e)$$

Equations (7) and (13) represent our TPP-2M formula for estimating IMFPs in other materials.

IMFPs calculated from the TPP-2M equation are shown in Figs 4–10 as dashed lines for each solid, and Table 6 shows values of the RMS deviations between these IMFPs and IMFPs calculated from optical data. The average RMS deviation for the 41 elemental solids over the 50 eV–30 keV range is 12.3%. This average deviation is almost the same as that found in a similar comparison for the 50–2 000 eV range (12.8%). We see relatively large RMS deviations for diamond, graphite, and cesium in Table 6 (71.7, 47.9 and 36.7%, respectively); reasons for these large deviations have been discussed in a previous paper.[10] If the RMS deviations for diamond, graphite, and cesium are ignored, the average RMS deviation for the remaining elements is 9.2%. This value is slightly better than the corresponding average RMS deviation of 10.2% found with IMFPs for the 50–2000 eV range for our original group of 27 elements.[7] We searched for but did not

SURFACE and INTERFACE ANALYSIS

Table 6. Root-mean-square (RMS) deviations between IMFPs from the TPP-2M equation [Eqns (7) and (13)] and IMFPs calculated from optical data for the indicated elemental solids and for energies between 50 eV and 30 keV

Element	RMS deviation (%)
Li	14.7
Be	23.7
C (graphite)	47.9
C (diamond)	71.7
C (glassy)	1.6
Na	4.6
Mg	9.0
Al	11.4
Si	3.0
K	2.1
Sc	24.8
Ti	20.6
V	8.2
Cr	5.8
Fe	2.6
Co	6.7
Ni	7.2
Cu	11.9
Ge	5.6
Y	14.3
Nb	2.9
Mo	6.6
Ru	4.3
Rh	6.2
Pd	4.4
Ag	8.2
In	20.6
Sn	4.9
Cs	36.7
Gd	6.6
Tb	11.4
Dy	5.3
Hf	12.9
Ta	17.0
W	8.8
Re	6.3
Os	6.6
Ir	6.6
Pt	9.1
Au	9.4
Bi	13.6

find any correlation between the RMS deviations in Table 6 and the sum-rule errors in Table 3. We also note that our calculated IMFPs for diamond are consistent with IMFPs determined from elastic-peak electron-spectroscopy (EPES) experiments by Zemek *et al*.[44] and the IMFP calculations of Rehr *et al*.[45] while our IMFPs for Cs are consistent with those calculated by Rehr *et al*.[45] In addition, Kunz *et al*.[46] analyzed XPS spectra of diamond and graphite that were obtained with 8 keV X-rays and found that the ratio of the IMFPs of diamond and graphite was 0.95 (for an electron energy of 7 716 eV). This ratio is slightly larger than the corresponding ratio of our calculated IMFPs of 0.88. There remains, however,

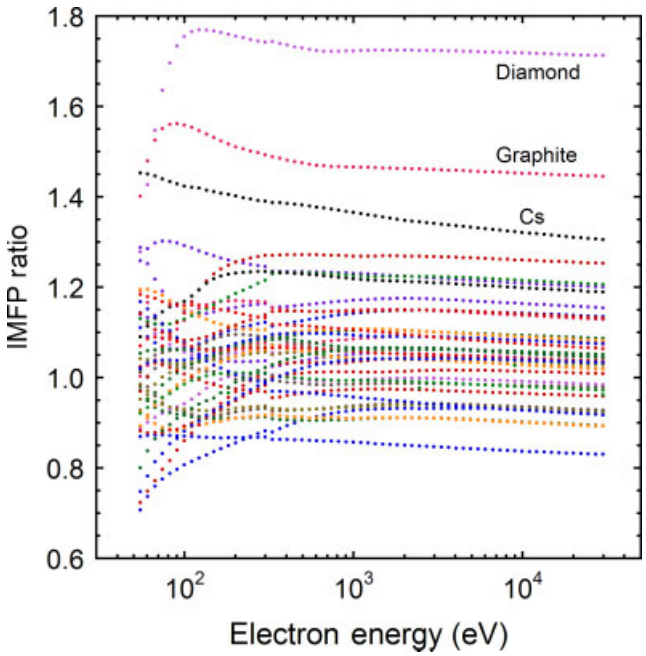

Figure 14. Ratio of IMFPs calculated from the TPP-2M equation [Eqns (7) and (13)] to IMFPs calculated from optical data as a function of electron energy for the 41 elemental solids.

an inconsistency between our IMFPs for graphite and the IMFPs from the EPES experiments of Tanuma *et al*.[47] (where the RMS difference was 27% for energies between 100 eV and 30 keV). The large RMS deviations for diamond and cesium (and probably also the RMS deviation for graphite) in Table 6 are believed to be due mainly to limitations of the TPP-2M formula, as discussed in Ref. [10]. The large RMS deviation for graphite might also be due to its anisotropic optical properties; such anisotropies are neglected in the Penn algorithm.

Figure 14 shows a plot of ratios of IMFPs calculated from TPP-2M to IMFPs calculated from optical data for the 41 elemental solids as a function of electron energy in order to assess visually the reliability of the TPP-2M equation for energies up to 30 keV. Ideally, these ratios should not change with energy and should be close to unity. For the 41 solids, the ratios are nearly constant with energy for energies above 300 eV but there are often substantial changes at lower energies. For energies above 300 eV, values of the maximum of the IMFP ratio divided by the minimum of the IMFP ratio were less than 1.07 for the 41 solids, and the average of these values was 1.03. For energies between 50 eV and 300 eV, Fig. 14 indicates that the TPP-2M equation is less satisfactory in this energy range than at higher energies. We note that while the IMFP ratios for diamond, graphite, and Cs in Fig. 14 exceed 1.3 for all energies, the energy dependence of the TPP-2M equation is satisfactory for energies between 300 eV and 30 keV.

Discussion

We will make comparisons here of our calculated IMFPs with results from recent calculations and from experiments.

Calculated IMFPs

Powell and Jablonski[16] described methods for calculating IMFPs in solids and analyzed calculated IMFPs for seven elemental solids

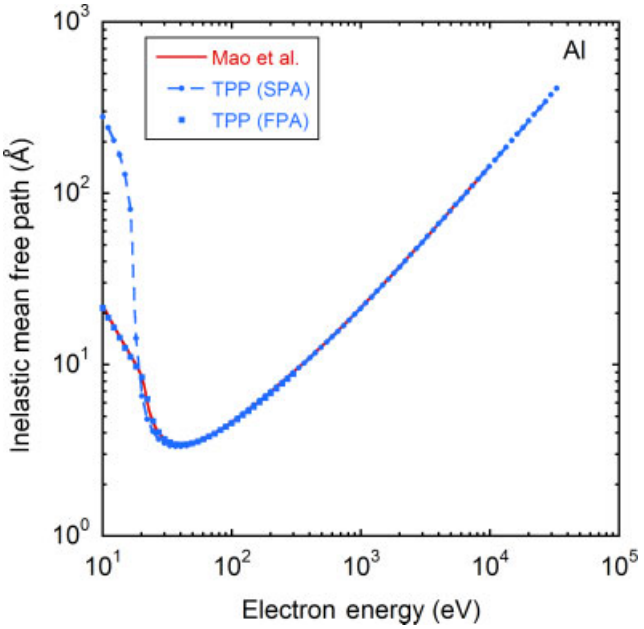

Figure 15. Comparison of IMFPs calculated from optical data for Al by Mao *et al*. (solid line, Refs. [48] and [49]) with our IMFPs that were obtained with the SPA [solid circles and dashed line, TPP (SPA)] and the full Penn algorithm [solid squares, TPP (FPA)].

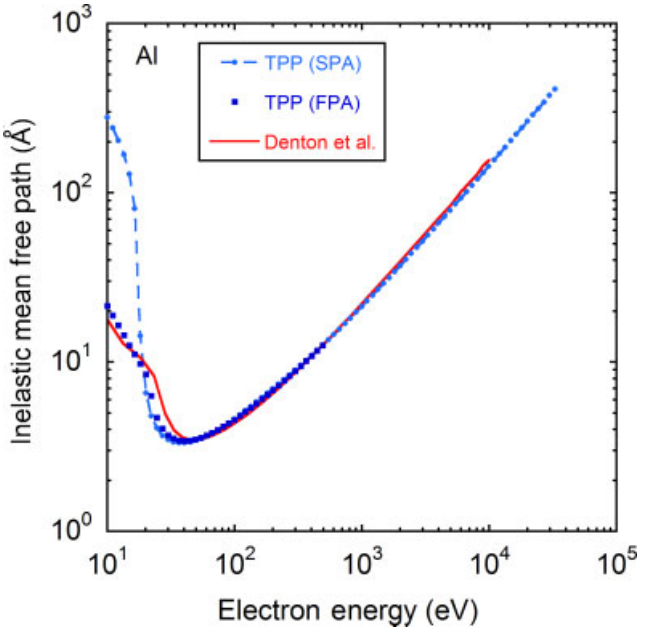

Figure 17. Comparison of IMFPs calculated from optical data for Al by Denton *et al*. (solid line, Ref. [38]) with our IMFPs that were obtained with the SPA [solid circles and dashed line, TPP (SPA)] and the full Penn algorithm [solid squares, TPP (FPA)].

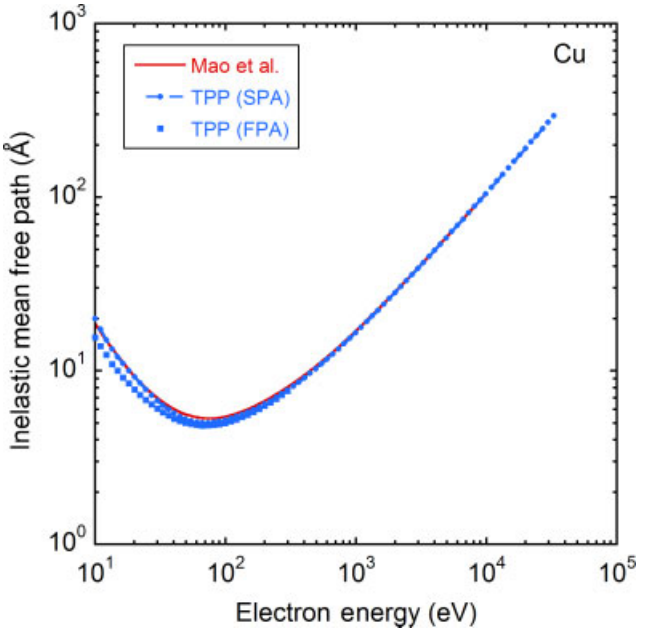

Figure 16. Comparison of IMFPs calculated from optical data for Cu by Mao *et al*. (solid line, Refs. [48] and [49]) with our IMFPs that were obtained with the SPA [solid circles and dashed line, TPP (SPA)] and the full Penn algorithm [solid squares, TPP (FPA)].

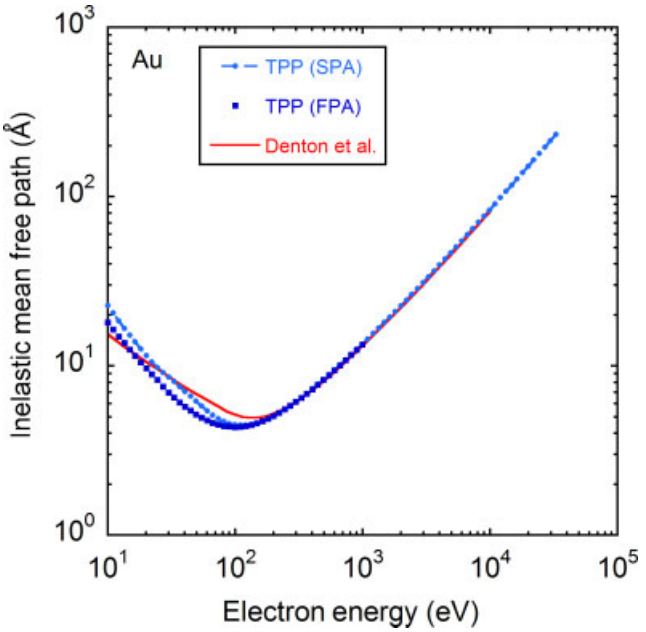

Figure 18. Comparison of IMFPs calculated from optical data for Au by Denton *et al*. (solid line, Ref. [38]) with our IMFPs that were obtained with the SPA [solid circles and dashed line, TPP (SPA)] and the full Penn algorithm [solid squares, TPP (FPA)].

(Al, Si, Ni, Cu, Ge, Ag and Au) for which there were at least two independent sources of IMFP calculations and IMFP measurements for each solid. The calculated IMFPs had been obtained from experimental optical data and algorithms generally similar to the Penn algorithm used here although different approaches were employed for selection and use of optical data and different technical approaches were chosen for the IMFP calculations. Nevertheless, the average RMS deviation of the calculated IMFPs from a function fitted to all of the calculated IMFPs for each of the seven solids was 4.4%.

We now discuss results from several groups that have commented recently on the Penn algorithm for IMFP calculations. Mao *et al*.[48,49] reported IMFPs for Al and Cu using two variations of the Penn algorithm, the so-called full Penn algorithm (FPA) and

the SPA. Calculations with the FPA are more time consuming than the SPA since the former requires a triple integration whereas the latter requires only a single integration. In our first major report of IMFPs for 27 elemental solids and electron energies between 200 eV and 2 keV,[3] we utilized the simpler SPA, Eqn (16) of Ref. [3], although in all later papers IMFPs were calculated with the FPA for electron energies between 50 eV and an upper limit of either 200 or 300 eV, as in Eqn (14) of Ref. [3]. Due to a misunderstanding, Mao *et al*.[48] initially claimed that the SPA was used for all of our IMFP calculations but this claim was later corrected.[49] Comparisons of our IMFPs calculated with the FPA and the SPA and of the Mao *et al*. IMFPs calculated with the FPA are shown in Figs 15 and 16 for Al and Cu, respectively. We see substantial differences in the IMFPs from the FPA and the SPA for Al at energies less than 20 eV in Fig. 15 and much smaller differences for Cu in Fig. 16. This result, previously reported by Mao *et al*., is associated with the strong and well-defined bulk-plasmon excitation in the energy-loss spectrum of Al and the neglect of single-electron excitations in the SPA.[48,50] There is excellent agreement in our FPA IMFPs for Al and those of Mao *et al*. in Fig. 15 and satisfactory agreement for Cu in Fig. 16. The slight differences for Cu at energies less than 100 eV are probably due to the selection of different sets of optical data in each calculation.

Denton *et al*.[38] reported IMFP calculations for Al and Au that were based on the use of a function proposed by Mermin[51] for describing outer-electron excitations. The Mermin function is an improvement over the Lindhard[20] dielectric function utilized in the Penn algorithm in that it accounts for the finite lifetimes of the various excitations. The ELF due to outer-electron excitations is obtained from experimental optical data, as in our work, and is typically represented by a sum of Mermin functions describing the positions, strengths, and widths of contributing excitations. The ELF for Al outer-shell excitations is based on Mermin functions for describing valence-band and L-shell excitations while the ELF for Au outer-shell excitations makes use of Mermin functions for valence-band and N-shell excitations, as per C. D. Denton and I. Abril (private communication). The contributions to the ELFs from inner-shell excitations were represented by generalized oscillator strengths for isolated atoms with parameters related to experimental data.[38] Denton *et al*. report that the parameters in their fits to the Al and Au optical ELFs were chosen in such a way that the fitted ELF reproduced the main trends of the optical ELF and satisfied the f-sum rule [Eqn (5)] for each solid.

Denton *et al*.[38] report significant differences (in their Fig. 7) between their IMFPs for Al and Au and those they show as coming from the 'Penn model' for electron energies less than about 30 eV for Al and about 100 eV for Au. We will now discuss these differences.

Figures 17 and 18 show comparisons of the Denton *et al*. IMFPs for Al and Au with our results from both the FPA and the SPA. For Al, we see a generally high degree of consistency in Fig. 17 between our results from the FPA and the Denton *et al*. IMFPs but with some differences between 20 eV and 40 eV. For Au, we find much closer agreement between IMFPs from the FPA and SPA in Fig. 18 at energies below 100 eV than for Al (as for Cu in Fig. 16). We also see good consistency of our IMFPs from the FPA with the Denton *et al*. IMFPs for energies above 200 eV, and small but systematic differences at lower energies. The latter differences are much smaller than those shown by Denton *et al*.; for example, at 20 eV, Denton *et al*. show IMFPs from the 'Penn model' as being more than twice those from their own calculations whereas our IMFPs are about 10% larger than those of Denton *et al*. The largest difference between our FPA IMFPs and those of Denton *et al*. occurred at energies between 50 and 60 eV where the difference was 32%.

The large differences shown by Denton *et al*. between their IMFPs and those from the 'Penn model' for energies less than about 40 eV for Al and about 200 eV for Au probably arise from their use of the SPA for their evaluation of the latter IMFPs and/or from use of a different dispersion relation. We do not expect the SPA to be reliable for such low electron energies.[1,2] Ding and Shimizu[52] found that IMFP calculations from the SPA using optical data and a simple dispersion relation (in which the energy loss varied as the square of the momentum transfer) led to IMFPs for Ni, Cu, Ag, and Au that were up to approximately twice those found with Eqn 3(b) for energies between 10 and 100 eV. A similar comparison for Si showed substantial increases in the IMFPs for the simple dispersion relation from values with Eqn 3(b) for energies less than about 30 eV. Their SPA results with the simple dispersion relation for Au and Si are similar to those reported by Denton *et al*. as resulting from the 'Penn model'. We note that Ding and Shimizu[53] later reported small decreases of IMFPs for Cu and Au with the SPA and the simple dispersion relation compared to those found with Eqn 3(b) but these results were incorrect, as per Z. J. Ding (private communication).

De la Cruz and Yubero[37] used a similar Mermin description of the dielectric function to calculate IMFPs of Si, Ti, Ag and Au for electron energies between 200 and 2 keV. They do not present numerical values of their IMFPs but show in their Fig. 2 that their IMFPs are systematically smaller than those from 'Penn's approach'. While the differences vary with material, the largest occur for Au and range from about 7.5% at 2 keV to about 14% at 200 eV. In the comparison of our IMFPs for Au with those obtained in the later work of Denton *et al*.[38] (Fig. 18), the latter IMFPs were slightly larger than our results with both the FPA and SPA at 200 eV. The differences in the energy dependences of the IMFPs found by de la Cruz and Yubero and by Denton *et al*. may have resulted from the neglect of inner-shell excitations and to smaller integration limits in the IMFP calculations of the former authors, as per F. Yubero (private communication). We also note that the comparison by de la Cruz and Yubero with 'Penn's approach' is based on an IMFP calculation with the SPA and a simple quadratic dispersion relation. Ding and Shimizu,[53] however, found that IMFPs with the quadratic dispersion relation for Au at 200 eV were larger by about 10% than those obtained with the quartic dispersion relation.

Emfietzoglou *et al*.[39] calculated IMFPs for liquid water, solid-DNA, and polymethylmethacrylate (PMMA) using different many-body local-field corrections to the Lindhard dielectric response function. They considered corrections proposed by Hubbard[54] (for exchange), Geldart and Vosko[55] (for exchange), Rice[56] (for screened exchange), Kleinman[57] and Langreth[58] (for exchange and correlation), and Corradini *et al*.[59] (for exchange and correlation). The latter correction formula was believed to be the most reliable and is widely used in time-dependent density functional theory.[39] Emfietzoglou *et al*. report that inclusion of the Corradini *et al*. exchange and correlation correction results in decreases of IMFPs for liquid water of about 10% for electron energies above 100 eV and of up to about 25% for energies between 10 and 100 eV compared to IMFPs evaluated from the full Lindhard dielectric function. The exchange and correlation corrections tested by Emfietzoglou *et al*. were applied to the screening electrons rather than to the energetic electron and, as a result, the screening is weaker and the IMFPs smaller as per D. Emfietzoglou (private communication).

We note that other groups have used different types of exchange corrections in their IMFP calculations, as discussed by Powell and Jablonski who estimated that consideration of exchange for the energetic electron would increase IMFPs by between about 10 and 15% for electron energies between 50 and 100 eV.[16] Tan *et al*.[60] compared IMFPs for a group of ten organic compounds that had been calculated from the SPA without an exchange correction and with exchange corrections based on two models, one a formalism proposed by Ashley and Anderson[61] and the other a modified Born-Ochkur approximation.[62,63] Inclusion of exchange led to IMFP increases of about 25% for the Ashley-Anderson model and about 18% for the modified Born-Ochkur model at an electron energy of 100 eV. The IMFP increases for an energy of 50 eV were about 43 and 34%, respectively. We note that Tan *et al*. used a simple quadratic dispersion relation and that their results would probably be different if they had chosen Eqn 3(b).

Finally, we wish to point out that there have been a number of first-principles calculations of IMFPs for energies less than about 50 eV,[64,65,66] as reviewed by Echenique *et al*.[67,68] These calculations are based on *ab initio* local-density theory in which the wave functions and corresponding energy for a given material are determined and then a dielectric function is calculated from that information. A self-consistent pseudopotential method with the local density approximation is used to obtain the exchange-correlation potential.[69] The resulting dielectric function can be very sensitive to the wave functions and energy levels of the material, i.e. to details of the band structure. The calculated IMFPs agree reasonably well with results of analyses of intensities for surface-shifted and nonsurface-shifted core-level photoelectron peaks of the alkali metals, Be, and Si.[69,70,71] The latter experiments provide a measure of what is now known as the effective attenuation length (EAL) which, for photoelectron emission angles less than about 60°, is less than the corresponding IMFP.[1] The importance of band-structure effects and of an integrated approach for correlation and exchange has been shown in the results of similar *ab initio* calculations of the dielectric function, hot-electron lifetimes, plasmon dispersion relations, and dynamical structure factors that also agree well with experiment.[71,72,72,73,74,75,76,77,78] While the approach used by Emfietzoglou *et al*.[39] of combining many-body exchange and correlation effects in an *ad hoc* manner with a phenomenological dielectric function may be viable for electron energies larger than about 50 eV, we believe that questionable results will be obtained for lower energies.[68–82]

IMFPs from Experiments

Elastic-peak electron spectroscopy (EPES) has been identified as the preferred experimental technique for determination of IMFPs.[16] Measurements are typically made of ratios of intensities of elastically backscattered electrons for the sample of interest and a selected reference sample for a range of electron energies, and these ratios are compared with corresponding ratios from a model calculation in which the IMFP of the sample is a parameter and the IMFP of the reference sample is chosen from a reference source.[16,17] We compare our calculated IMFPs with values from the EPES experiments of two groups who reported IMFPs for a large number of elemental solids.[47] Sources of uncertainty in IMFPs from EPES experiments are discussed elsewhere.[1,16]

Tanuma *et al*. determined IMFPs by EPES for 13 elemental solids (graphite, Si, Cr, Fe, Cu, Zn, Ga, Mo, Ag, Ta, W, Pt and Au) and electron energies between 50 eV and 5 keV using a Ni reference sample.[47] They also fitted the Bethe equation (Eqn (7) with $C = D = 0$) to their IMFPs for energies greater than 100 eV. The Bethe equation can be rewritten as:

$$E/\lambda = E_P^2 \beta \ln(\gamma E) \tag{14}$$

It is then straightforward to determine values of β and γ from Fano plots in which E/λ is plotted versus ln E. Werner *et al*. similarly determined IMFPs from EPES experiments for 24 elemental solids (Ag, Al, Au, Be, Bi, C, Co, Cu, Fe, Ge, Mg, Mn, Mo, Ni, Ta, Te, Ti, Pb, Pd, Pt, Si, V, W, Zn) for energies between 50 and 3400 eV. Their IMFPs were averages of values obtained with respect to Ni, Cu, Ag and Au reference samples or, in the case of these four solids, to use of the other three as reference materials. Werner *et al*. similarly obtained β and γ values from Fano plots for energies above 200 eV.[79,80]

We have compared our calculated IMFPs for those elemental solids that are common to the EPES measurements of Tanuma *et al*. (11 solids) and of Werner *et al*. (17 solids). In these comparisons, IMFPs were computed from Eqn (14) and the values of β and γ reported by each group. Figures 19–23 show examples of our comparisons for graphite, Si, Fe, Ag and Au in the form of Fano plots. In each Figure, we show Fano plots with our calculated IMFPs ('optical' IMFPs), with IMFPs from the TPP-2M equation [Eqns (7) and (13)], and with IMFPs from the Tanuma *et al*. and Werner *et al*. experiments. For graphite (Fig. 19), we see that the Fano plots with the optical IMFPs are systematically larger than those with IMFPs from other sources.[10] The slope of the Fano plot for the IMFPs from the TPP-2M equation, however, is in good agreement with those for IMFPs from both EPES results. In Figs 20 (for Si) and 21 (for Fe), the optical IMFPs are in good agreement with those from the TPP-2M equation and both EPES measurements although the slope of the Fano plot from the Werner *et al*. EPES data for Si differs slightly from the other plots and the slope of the Fano plot from the Tanuma *et al*. EPES data for Fe differs from the other plots. For Ag (Fig. 22) and Au (Fig. 23), the optical IMFPs agree well with those from the TPP-2M equation and from the EPES experiments of Tanuma *et al*. There are small but systematic differences with some of the IMFPs from the Werner *et al*. experiments, with the slopes of the Fano plots for Ag and Au from the latter IMFPs being slightly larger (for Ag) or smaller (for Au) than found for the other IMFPs.

Although there are some inconsistencies in the comparisons shown in Figs 19–23 (particularly for graphite), we conclude from the general overall agreement in the slopes of the Fano plots that the energy dependences of the EPES IMFPs is very similar to the energy dependences of the optical IMFPs. We note that the EPES IMFPs described here were obtained from comparative measurements in which elastic-backscattered intensities from the sample of interest were compared with similar intensities from a reference material (Ni for the Tanuma *et al*. experiments and generally Ni, Cu, Ag and Au for the Werner *et al*. experiments). As a result, the ratios of intensities may have only a weak dependence on the primary-electron energy. Nevertheless, there is no evidence of significant differences in the Fano-plot slopes for Si in Fig. 20 or of changes in these slopes with electron energy that might arise from the dissimilar electronic properties of Si (a free-electron-like solid) and Ni (a transition metal). In principle, the dissimilar electronic properties could cause differences between the Fano-plot slopes for the EPES IMFPs and the optical IMFPs at low electron energies (particularly close to 100 eV) due to different probabilities for surface-electronic excitations (discussed below) or to correlation and exchange corrections (discussed above).

SURFACE and INTERFACE ANALYSIS

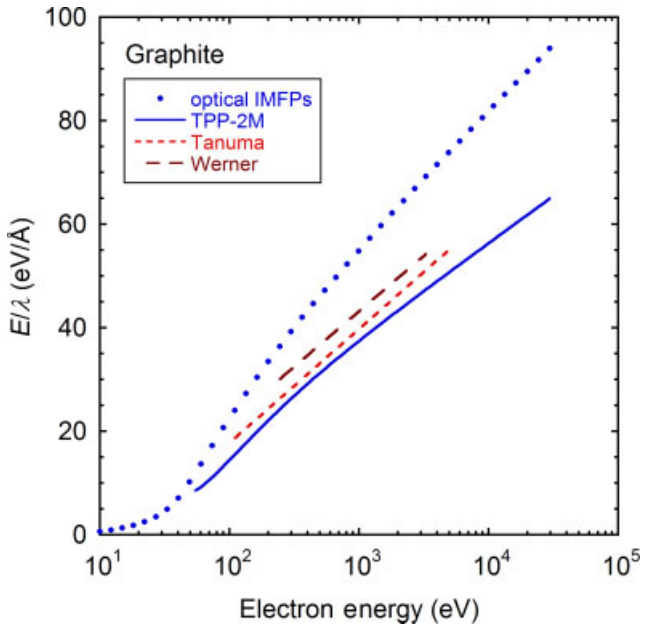

Figure 19. Comparison of Fano plots for graphite with E/λ plotted as a function of electron energy. The solid circles are values of E/λ with IMFPs from our optical IMFPs. The solid line indicates values of E/λ with IMFPs calculated from the TPP-2M equation [Eqns (7) and (13)]. The dashed and dotted lines show E/λ values from IMFPs calculated with Eqn (14) using parameters obtained from the EPES experiments of Tanuma *et al*. (Ref. [47]) and Werner *et al*. (Refs. [83] and [84]), respectively.

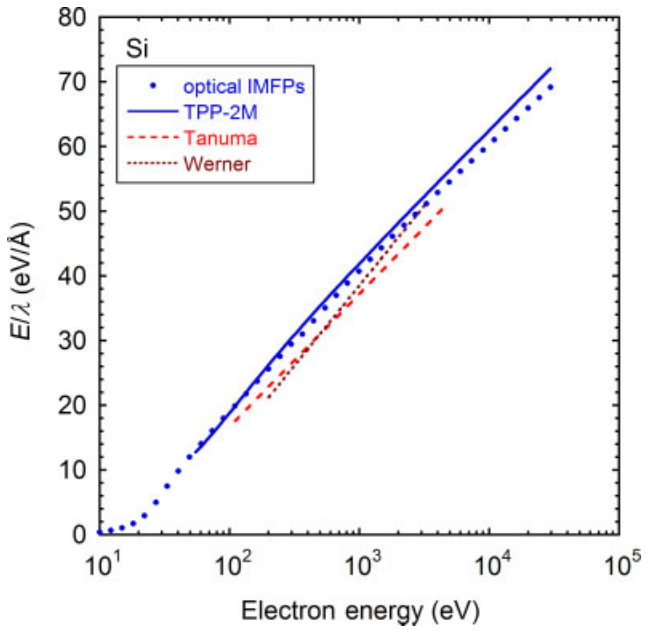

Figure 20. Comparison of Fano plots for silicon with E/λ plotted as a function of electron energy. See caption to Fig. 18.

There is, however, a significant difference in the Fano-plot slopes for the optical IMFPs and the IMFPs from the EPES experiments for graphite in Fig. 19. We speculate that this difference might be associated with the highly anisotropic optical properties of graphite. Our ELF data was obtained from the electron energy-loss spectroscopy experiments of Venghaus[81] who reported the ELF for momentum transfers perpendicular to the graphite *c*-axis. The

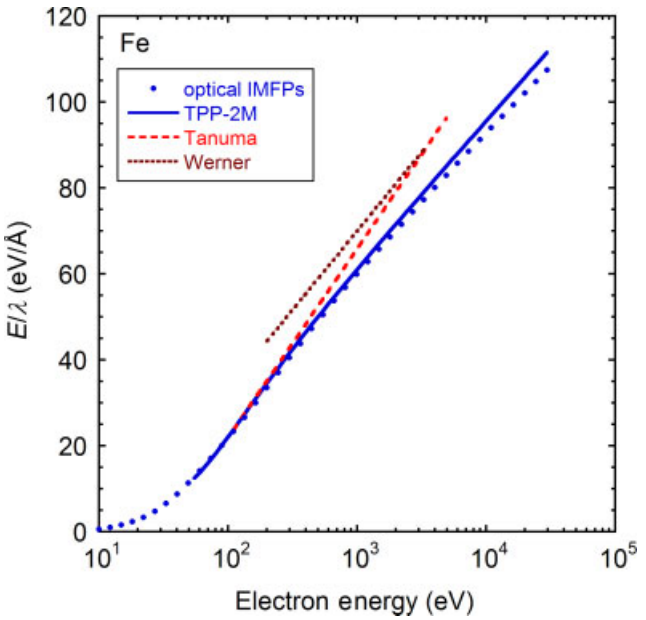

Figure 21. Comparison of Fano plots for iron with E/λ plotted as a function of electron energy. See caption to Fig. 18.

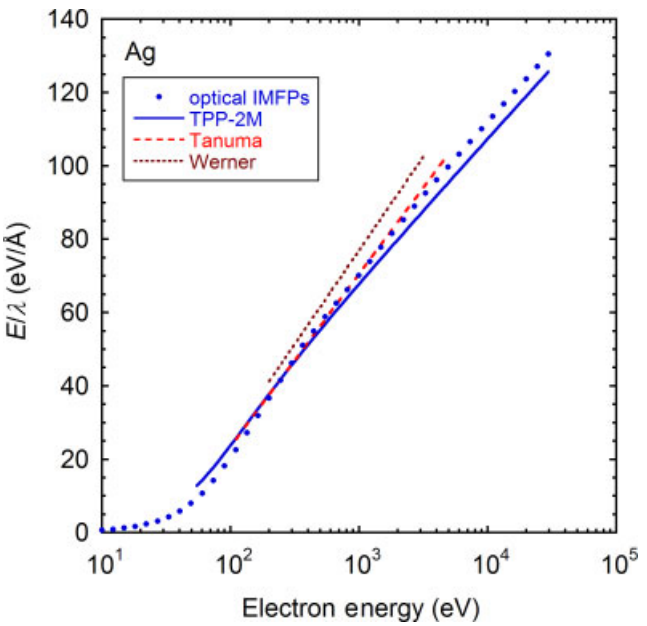

Figure 22. Comparison of Fano plots for silver with E/λ plotted as a function of electron energy. See caption to Fig. 18.

ELF for momentum transfers parallel to the *c*-axis has a different shape.[36] The Penn algorithm was developed for isotropic solids, and it is likely that our optical IMFPs for graphite have much larger uncertainties than for the other elemental solids. We also note that the graphite samples used in the Tanuma *et al*. EPES experiments were not sputtered, and thus the resulting IMFPs could have some error arising from diffraction effects (there was some waviness in the original Fano plot for the graphite IMFPs[47]). Nevertheless, the graphite sample used by Werner *et al*. was sputtered and the slope of the resulting Fano plot was essentially identical to that reported by Tanuma *et al*., as shown in Fig. 19.

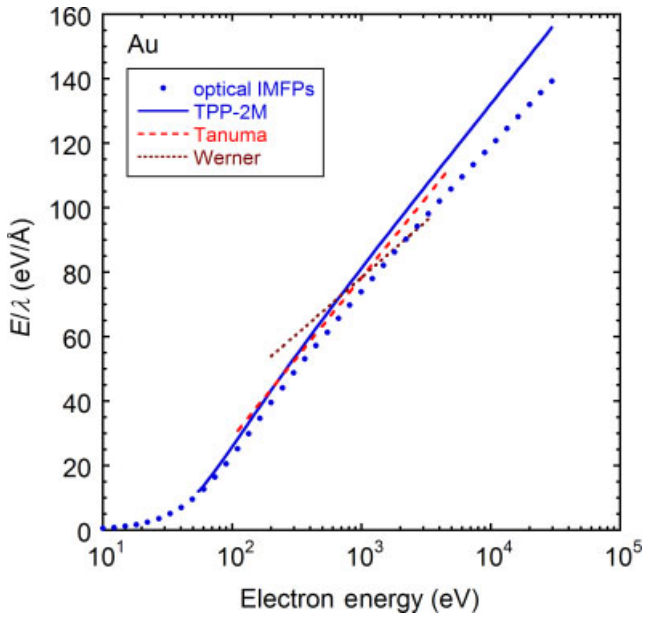

Figure 23. Comparison of Fano plots for gold with E/λ plotted as a function of electron energy. See caption to Fig. 18.

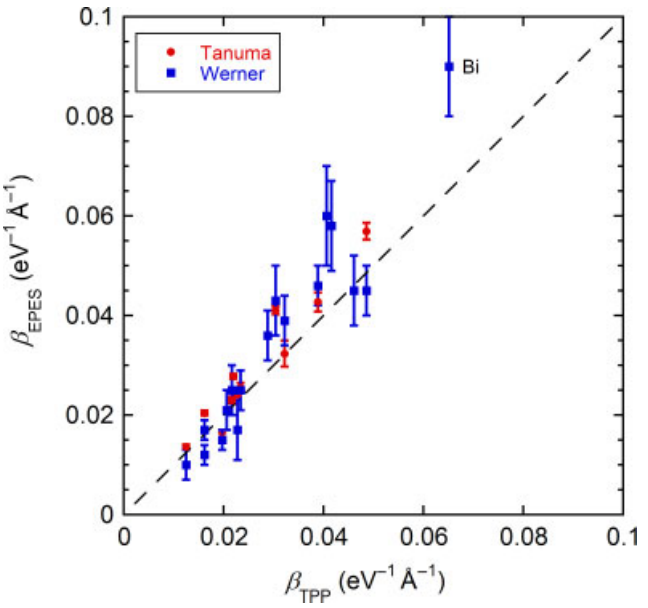

Figure 24. Plot of β_{EPES} values from the EPES experiments of Tanuma *et al*. (Ref. [47], solid circles) and Werner *et al*. (Refs. [83] and [84], solid squares) versus values of β_{TPP} from Eqn (15) (evaluated with parameter values from Table 5 and for an energy of 1 keV) for the elemental solids common to our calculations and each set of EPES measurements.

We calculated RMS differences between our optical IMFPs and the IMFPs from the EPES results of Tanuma *et al*. and Werner *et al*. for the common solids in each comparison. IMFPs were computed for the same energies as our calculations between 100 eV and 5 000 eV for the Tanuma *et al*. comparison and between 200 and 3 400 eV for the Werner *et al*. comparison. We also made similar comparisons between IMFPs from the TPP-2M equation and the IMFPs from the EPES measurements. The average RMS differences were 12% (11 elemental solids) for the comparison of the optical IMFPs with the Tanuma *et al*. IMFPs and 11% (13 elemental solids) for the comparison of the TPP-2M IMFPs and the Tanuma *et al*. IMFPs. We similarly found average RMS differences of 15% (17 elemental solids) for the comparison of optical IMFPs with the Werner *et al*. IMFPs and 19% (17 elemental solids) for the comparison of the TPP-2M IMFPs and the Werner *et al*. IMFPs. The relatively large RMS differences in the latter comparisons are associated with the relatively large uncertainties of the parameters β and γ reported by Werner *et al*.[83,84]

Values of IMFPs from the Bethe equation [Eqn (14)] are mainly determined by the value of β which can be obtained from the slope of a Fano plot. We now compare β values obtained from Fano plots with IMFPs from the EPES measurements of Tanuma *et al*. and Werner *et al*., β_{EPES}, to similar values obtained from analyses of our calculated IMFPs. We have already shown in Figs 12 and 13 that the slopes of Fano plots, as evaluated from Eqns (10), (11) and (12), are functions of energy. Values of β_{EPES}, however, were determined as average slopes over moderately large energy ranges (100 eV–5 keV for the Tanuma *et al*. IMFPs, and 200 eV–3.4 keV for the Werner *et al*. IMFPs). We have chosen to compare values of β_{EPES} from each data source with values of β_{TPP} that were obtained from the slopes of Fano plots with our optical IMFPs using Eqn (12),

$$\beta_{TPP} = \beta + (C/E) - (2D/E^2), \qquad (15)$$

and with Eqn (15) evaluated at an energy of 1 keV and values of β, C, and D from Table 5. Figure 24 shows plots of β_{EPES} from each data source versus β_{TPP} for the elemental solids that are common to the EPES measurements and our calculations. We see that there is a generally satisfactory correlation between the β_{EPES} values from the Tanuma *et al*. EPES measurements (solid circles) and values of β_{TPP} (as represented by the dashed line $\beta_{EPES} = \beta_{TPP}$. There is also a reasonable correlation between the β_{EPES} values from the Werner *et al*. measurements (solid squares) and β_{TPP} although one data point (for Bi) appears to be an outlier.

Powell and Jablonski[16] have discussed the following sources of uncertainty in IMFPs from EPES measurements: (i) validity of the theoretical model describing the elastic-backscattering probability; (ii) technique for measuring the elastic-peak intensity; (iii) IMFP values for the reference material; (iv) surface excitations; (v) surface roughness; (vi) surface composition (e.g. presence of any surface contamination); (vii) specimen crystallinity; and (viii) stability of the primary-beam current. IMFPs from most EPES experiments are based on ratios of elastically scattered intensities at a given energy for two materials, the sample of interest and a reference sample.[1,16] The experimental ratios are compared with similar ratios obtained from Monte Carlo simulations. The latter ratios depend on the reliability of calculated differential elastic-scattering cross-sections and other parameters. Although the cross sections may have significant uncertainties,[82,83] the calculated intensity ratios should have much smaller uncertainties.

The EPES IMFPs of Tanuma *et al*. and Werner *et al*. were based on relative measurements of elastically backscattered intensities for each sample to similar measurements for one or more reference solids for which the IMFPs were believed known. These reference solids (Ni, Cu, Ag and Au) were those identified by Powell and Jablonski as materials with 'recommended' values of IMFPs that were based, for each solid, on calculated IMFPs from two or more groups that showed a high degree of consistency with each other and with IMFPs from EPES experiments (also from two or more groups). More recently, Powell and Jablonski[1] concluded that IMFPs calculated from optical data have uncertainties of

SURFACE and INTERFACE ANALYSIS

up to about 10%. We therefore believe that there is satisfactory consistency between our optical IMFPs and the IMFPs from the experiments of Tanuma *et al*. and Werner *et al*.

Finally, we mention briefly several further tests of IMFPs calculated from optical data. Seah *et al*.[84] made an extensive comparison of measured AES and XPS peak intensities with corresponding calculated peak intensities for some 60 elemental solids. One parameter in these calculations was the IMFP, and Seah *et al*. chose to use IMFPs from the TPP-2M equation. They found good agreement between the measured and calculated intensities, with scatter factors of about 1.09 for AES and about 1.12 for XPS. For a careful analysis of thicknesses of thin films of SiO_2 on Si determined by XPS and other techniques, Seah and Spencer[85] determined the effective attenuation lengths (EALs) of Si 2p photoelectrons in SiO_2. Their EALs, 2.996 and 3.485 nm for XPS with Mg Kα and Al Kα X-ray sources, respectively, agreed well with the corresponding calculated values of 2.76 and 3.21 nm.[86] The latter values are based on average IMFP values at each photoelectron energy for Si and SiO_2 from previously reported IMFP calculations[4,5] and a correction for the effects of elastic scattering.[87]

Werner *et al*.[27] recently analyzed REELS of 17 elemental metals to determine optical constants for photon energies between 0.5 and 70.5 eV that, with atomic photoabsorption data for higher photon energies, were utilized to calculate IMFPs with Penn's algorithm.[18] For these 17 solids, the average RMS deviation of these IMFPs for energies between 99.5 and 9897.1 eV and our IMFPs in Table 4 was 5.9%. Werner *et al*. also commented that IMFPs from their REELS data were 'indistinguishably similar' to those obtained from parallel calculations of optical constants using density-functional theory. Given the uncertainties of the optical data used in our IMFP calculations (Table 3) and the uncertainties in IMFP calculations from optical data (~10%),[1,16] there is satisfactory consistency of our IMFPs with those obtained from other methods.

Conclusion

We report new calculations of IMFPs for 41 elemental solids (Li, Be, graphite, diamond, glassy C, Na, Mg, Al, Si, K, Sc, Ti, V, Cr, Fe, Co, Ni, Cu, Ge, Y, Nb, Mo, Ru, Rh, Pd, Ag, In, Sn, Cs, Gd, Tb, Dy, Hf, Ta, W, Re, Os, Ir, Pt, Au and Bi) for electron energies from 50 eV to 30 keV. The IMFPs were calculated from experimental optical data using the full Penn algorithm for energies up to 300 eV and the simpler SPA for higher energies. Improved sets of optical data over those used for our previous IMFP calculations[3,4] were utilized for 21 of the solids (Mg, Ti, V, Cr, Fe, Ni, Cu, Y, Nb, Mo, Ru, Rh, Pd, Hf, Ta, W, Re, Os, Ir, Pt and Au).

Figure 25 is a summary plot of the calculated IMFPs for the 41 solids as a function of energy. IMFPs are shown for energies between 10 and 50 eV to indicate trends but these values are not as reliable as those at higher energies. For energies between 1 and 30 keV, there is at least a factor of five difference between the smallest and largest IMFPs. Such variations in IMFP magnitudes are due mainly to variations in bulk densities. Minima in the IMFP plots occur at energies between about 10 and 100 eV. These variations are associated with differences in the shapes of the energy-loss functions for the solids.[40]

The calculated IMFPs could be fitted to the modified Bethe equation for inelastic scattering of electrons in matter for energies from 50 eV to 30 keV. The average RMS deviation in these fits

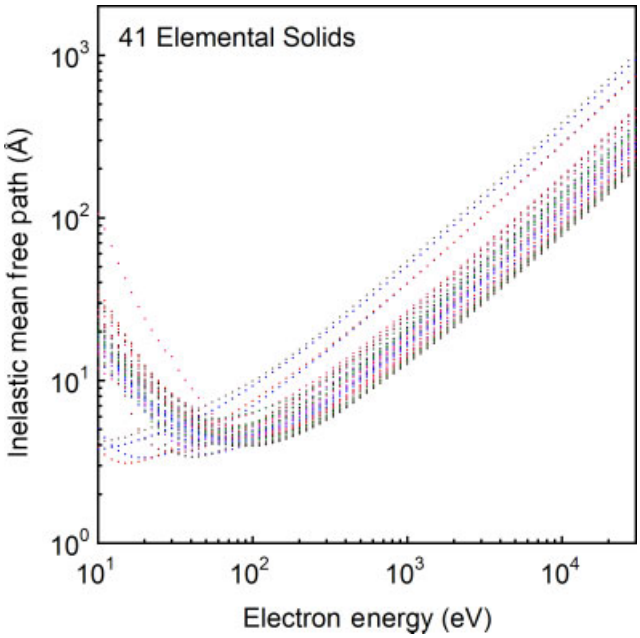

Figure 25. Summary plot of calculated IMFPs for the 41 elemental solids (Table 4) as a function of electron energy.

was 0.48%. We also compared the calculated IMFPs with values from the predictive TPP-2M equation [Eqns (7) and (13)] which was developed from our earlier IMFP calculations for the 50 eV–2 keV range. The average RMS deviation in this comparison for the 41 solids was 12.3%; this average RMS deviation was almost the same as that found in a similar comparison for the 50 eV–2 keV range (12.8%). Large RMS deviations were found for diamond, graphite, and cesium (71.7, 47.9 and 36.7%, respectively) as shown in Table 6; possible reasons for these large deviations were discussed in a previous paper.[10] If the RMS deviations for diamond, graphite and cesium are excluded, the average RMS deviation for the remaining 38 elements is 9.2%. This value is slightly superior to the corresponding average RMS deviation of 10.2% found with IMFPs for the 50 eV–2 keV range for our original group of 27 elemental solids.[7] The large deviations between the calculated IMFPs and those from the TPP-2M equation for diamond, graphite and cesium were traced to the relatively small computed values of the parameter β in the TPP-2M equation [from Eqn (13(b))] ($\beta \approx 0.01$ for diamond and graphite) and also for relatively large values of β ($\beta \approx 0.25$ for Cs).[10] Other solids may have similarly low values of β (as indicated by the values from the fits of Eqn (7) to the calculated IMFPs in Table 5) but, for their particular material parameters, there was less sensitivity of the IMFPs from TPP-2M than for diamond and graphite. We also note that the large deviation for graphite could be associated with the highly anisotropic optical properties of graphite; such anisotropies are neglected in the Penn algorithm. We therefore believe that the TPP-2M equation should be useful for estimating IMFPs in most materials for electron energies up to 30 keV in most materials with an average RMS uncertainty of about 10%. Larger uncertainties may occur for energies less than 300 eV.

We have compared our calculated IMFPs with those from other recent calculations and from experiments. Our results for Al and Cu agree well with those of Mao *et al*.[48,49] who also used the FPA. There is also generally good consistency between our results for Al

and Au and those of Denton *et al*.[38] who used Mermin functions to describe outer-electron excitations rather than the Lindhard function that was utilized in the Penn algorithm. Comparisons were also made with IMFPs determined by elastic-peak electron spectroscopy that were reported by Tanuma *et al*.[47] for 11 elemental solids and by Werner *et al*.[83,84] for 17 elemental solids. Satisfactory agreement was found in most of these comparisons. The average RMS differences between the calculated IMFPs and the experimental IMFPs were 12% for the Tanuma *et al*. results and 15% for the Werner *et al*. results.

Acknowledgments

We thank Drs I. Abril, C. D. Denton, Z.-Y. Ding, D. Emfietzoglou, J. J. Kas, L. Kover, J. J. Rehr, J. S. Villarrubia, W. S. M. Werner and F. Yubero for useful comments and discussions; and Drs Denton, Ding, Kas, Rehr, Werner and Yubero for supplying numerical data.

References

[1] C. J. Powell, A. Jablonski, *Nucl. Instr. Methods Phys. Res. A.* **2009**, *54*, 601.
[2] C. J. Powell, A. Jablonski A, *J. Electron Spectrosc. Relat. Phenom.* (in press).
[3] S. Tanuma, C. J. Powell, D. R. Penn, *Surf. Interface Anal.* **1988**, *11*, 577.
[4] S. Tanuma, C. J. Powell, D. R. Penn, *Surf. Interface Anal.* **1991**, *17*, 911.
[5] S. Tanuma, C. J. Powell, D. R. Penn, *Surf. Interface Anal.* **1991**, *17*, 929.
[6] S. Tanuma, C. J. Powell, D. R. Penn, *Surf. Interface Anal.* **1993**, *20*, 77.
[7] S. Tanuma, C. J. Powell, D. R. Penn, *Surf. Interface Anal.* **1994**, *21*, 165.
[8] S. Tanuma, C. J. Powell, D. R. Penn, *Surf. Interface Anal.* **1997**, *25*, 25.
[9] S. Tanuma, C. J. Powell, D. R. Penn, *Surf. Interface Anal.* **2003**, *35*, 268.
[10] S. Tanuma, C. J. Powell, D. R. Penn, *Surf. Interface Anal.* **2005**, *37*, 1.
[11] S. Tanuma, C. J. Powell, D. R. Penn, *J. Electron Spectrosc. Relat. Phenom.* **1993**, *62*, 95.
[12] H. Bethe, *Ann. Phys.* **1930**, *5*, 325.
[13] C. S. Fadley, *Nucl. Instr. Methods Phys. Res. A.* **2005**, *24*, 547.
[14] W. S. M. Werner, L. Kover, J. Toth, D. Varga, *J. Electron Spectrosc. Relat. Phenom.* **2002**, *103*, 122.
[15] G. Beamson, N. Moslemzadeh, P. Weightman, J. F. Watts, *J. Electron Spectrosc. Relat. Phenom.* **2008**, *19*, 162.
[16] C. J. Powell, A. Jablonski, *J. Phys. Chem. Ref. Data* **1999**, *19*, 28.
[17] G. Gergely, *Prog. Surf. Sci.* **2002**, *31*, 71.
[18] D. R. Penn, *Phys. Rev. B* **1987**, *35*, 482.
[19] D. R. Penn, *Phys. Rev. B* **1976**, *13*, 5248.
[20] J. Lindhard, *K. Dan. Vidensk. Selsk. Mat.-Fys. Medd.* **1954**, *28*, 1.
[21] H.-J. Hagemann, W. Gudat, C. Kunz, Deutsches Elektronen-Synchrotron Report SR-74/7, Hamburg 1974 unpublished; H.–J. Hagemann, W. Gudat, C. Kunz, *J. Opt. Soc. Am.* **1975**, *65*, 742.
[22] B. L. Henke, J. C. Davis, E. M. Gullikson, R. C. C. Perera, Lawrence Berkeley Laboratory Report 26259, 1988; B. L. Henke, E. M. Gullikson, J. C. Davis, *At. Data Nucl. Data Tables* **1993**, *54*, 181.
[23] E. D. Palik, *Handbook of Optical Constants of Solids*, Academic Press, New York, **1985**.
[24] E. D. Palik (ed.), *Handbook of Optical Constants of Solids III*, Academic Press, New York, **1998**.
[25] Y. A. Uspenskii, J. F. Seely, N. L. Popov, A. V. Vinogradov, Y. P. Pershin, V. V. Kondratenko, *J. Opt. Soc. Am. A* **2004**, *21*, 298.
[26] J. H. Weaver, C. Krafka, D. W. Lynch, E. E. Koch, *Optical Properties of Metals*, *Physik Daten*, Nos. 18-1 and 18-2, Fachinformationszentrum, Karlsruhe **1981**.
[27] W. S. M. Werner, K. Glantschnig, C. Ambrosch-Draxl, *J. Phys. Chem. Ref. Data* **2009**, *38*, 1013.
[28] B. L. Henke, P. Lee, T. J. Tanaka, R. L. Shimabukuro, B. K. Fujikawa, *Low Energy X-ray Diagnostics*, *Amer. Inst. Phys. Conf. Proc.* No. 75, American Institute of Physics, New York, **1981**.
[29] B. L. Henke, P. Lee, T. J. Tanaka, R. L. Shimabukuro, B. K. Fujikawa, *At. Data Nucl. Data Tables* **1982**, *27*, 1.
[30] E. D. Palik, *Handbook of Optical Constants of Solids II*, Academic Press, New York, **1991**.
[31] B. Brousseau-Lahaye, C. Colliex, J. Frandon, M. Casgnier, P. Trebbia, *Phys. Stat. Sol. (b)* **1975**, *69*, 257.
[32] J. L. Robins, J. B. Swan, *Proc. Phys. Soc. (London)* **1960**, *76*, 857.
[33] M. J. Lynch, J. B. Swan, *Aust. J. Phys.* **1968**, *21*, 811.
[34] C. Wehenkel, B. Gauthe, *Phys. Stat. Sol. (b)* **1974**, *64*, 515.
[35] M. Cukier, B. Gauthe, C. Wehenkel, *J. Physique* **1980**, *41*, 603.
[36] J. Daniels, C. v. Festenberg, H. Raether, K. Zeppenfeld, *Springer Tracts in Modern Physics* **1970**, *54*, 77.
[37] W. De la Cruz, F. Yubero, *Surf. Interface Anal.* **2007**, *39*, 460.
[38] C. D. Denton, I. Abril, R. Garcia-Molina, J. C. Moreno-Marin, S. Heredia-Avalos, *Surf. Interface Anal.* **2008**, *40*, 1481.
[39] D. Emfietzoglou, I. Kyriakou, I. Abril, R. Garcia-Molina, I. D. Petsalakis, H. Nikjoo, A. Pathak, *Nucl. Instr. Methods Phys. Res. B* **2009**, *267*, 45.
[40] S. Tanuma, C. J. Powell, D. R. Penn, *J. Electron Spectrosc. Relat. Phenom.* **1990**, *52*, 285.
[41] M. Inokuti, *Rev. Mod. Phys.* **1971**, *43*, 297.
[42] C. J. Powell, *Surf. Interface Anal.* **1987**, *10*, 349.
[43] U. Fano, *Phys. Rev.* **1954**, *95*, 1198.
[44] J. Zemek, J. Potmesil, M. Vanecek, B. Lesiak, A. Jablonski, *Appl. Phys. Letters* **2005**, *87*, 262114.
[45] J. J. Rehr, (private communication); http://leonardo.phys.washington.edu/feff/loss (accessed April 30, 2009).
[46] C. Kunz, B. C. C. Cowie, W. Drube, T.-L. Lee, S. Thiess, C. Wild, J. Zegenhagen, *J. Electron Spectrosc. Relat. Phenom.* **2009**, *173*, 29.
[47] S. Tanuma, T. Shiratori, T. Kimura, K. Goto, S. Ichimura, C. J. Powell, *Surf. Interface Anal.* **2005**, *37*, 833.
[48] S. F. Mao, Y. G. Li, R. G. Zeng, Z. J. Ding, *J. Appl. Phys.* **2008**, *104*, 114907.
[49] S. F. Mao, Y. G. Li, R. G. Zeng, Z. J. Ding, *J. Appl. Phys.* **2009**, *105*, 099902.
[50] K. O. Jensen, A. B. Walker, *Surf. Sci.* **1993**, *292*, 83.
[51] N. D. Mermin, *Phys. Rev. B* **1970**, *1*, 2362.
[52] Z. J. Ding, R. Shimizu, *Surf. Sci.* **1989**, *222*, 313.
[53] Z. J. Ding, R. Shimizu, *Scanning* **1996**, *18*, 92.
[54] J. Hubbard, *Proc. Roy. Soc. London A* **1958**, *243*, 336.
[55] D. J. W. Geldart, S. H. Vosko, *Can. J. Phys.* **1966**, *44*, 2137.
[56] T. M. Rice, *Ann. Phys.* **1965**, *31*, 100.
[57] L. Kleinman, *Phys. Rev.* **1967**, *160*, 585.
[58] D. C. Langreth, *Phys. Rev.* **1969**, *181*, 753.
[59] M. Corradini, R. Del Sole, G. Onida, M. Palumno, *Phys. Rev. B* **1998**, *57*, 14569.
[60] Z. Tan, Y. Xia, M. Zhao, X. Liu, F. Li, B. Huang, Y. Ji, *Nucl. Instr. Methods Phys. Res. B* **2004**, *222*, 27.
[61] J. C. Ashley, V. E. Anderson, *J. Electron Spectrosc. Relat. Phenom.* **1981**, *24*, 127.
[62] J. M. Fernandez-Varea, R. Mayol, D. Liljequist, F. Salvat, *J. Phys. Condens. Matter* **1993**, *5*, 3593.
[63] J. M. Fernandez-Varea, D. Liljequist, S. Csillag, R. Räty, F. Salvat, *Nucl. Instr. Methods Phys. Res. B* **1996**, *108*, 35.
[64] J. S. Dolado, V. M. Silkin, M. A. Cazalilla, A. Rubio, P. M. Echenique, *Phys. Rev. B* **2001**, *64*, 195128.
[65] V. M. Silkin, E. V. Chulkov, P. M. Echenique, *Phys. Rev. B* **2003**, *68*, 205106.
[66] V. P. Zhukov, E. V. Chulkov, P. M. Echenique, *Phys. Rev. B* **2006**, *73*, 125105.
[67] P. M. Echenique, J. M. Pitarke, E. V. Chulkov, A. Rubio, *Chem. Phys.* **2000**, *251*, 1.
[68] E. V. Chulkov, A. G. Borisov, J. P. Gauyacq, D. Sanchez-Portal, V. M. Silkin, V. P. Zhukov, P. M. Echenique, *Chem. Rev.* **2006**, *106*, 4160.
[69] N. V. Smith, G. K. Wertheim, A. B. Andrews, C.-T. Chen, *Surf. Sci. Letters* **1993**, *282*, L359.
[70] L. I. Johansson, B. E. Sernelius, *Phys. Rev. B* **1994**, *50*, 16817.
[71] T.-W. Pi, I.-H. Hong, C.-P. Cheng, G. K. Wertheim, *J. Electron Spectrosc. Relat. Phenom.* **2000**, *107*, 163.
[72] N. E. Maddocks, R. W. Godby, R. J. Needs, *Europhys. Lett.* **1994**, *27*, 681.
[73] N. E. Maddocks, R. W. Godby, R. J. Needs, *Phys. Rev. B* **1994**, *49*, 8502.
[74] M. Ehrnsperger, H. Bross, *J. Phys.: Condens. Matter* **1997**, *9*, 1225.
[75] S. Waidman, M. Knupfer, B. Arnold, J. Fink, A. Fleszar, W. Hanke, *Phys. Rev. B* **2000**, *61*, 10149.
[76] A. G. Marinopoulos, L. Reining, V. Olevano, A. Rubio, T. Pichler, X. Liu, M. Knupfer, J. Fink, *Phys. Rev. Letters* **2002**, *89*, 076402.
[77] I. G. Gurtubay, J. M. Pitarke, W. Ku, A. G. Eguiluz, B. C. Larson, J. Tischler, P. Zschack, K. D. Finkelstein, *Phys. Rev. B* **2005**, *72*, 125117.

[78] H.-C. Weissker, J. Serrano, S. Huotari, F. Bruneval, F. Sottile, G. Monaco, M. Krisch, V. Olevano, L. Reining, *Phys. Rev. Letters* **2006**, *97*, 237602.
[79] W. S. M. Werner, C. Tomastik, T. Cabela, G. Richter, H. Störi, *Surf. Sci.* **2000**, *470*, L123.
[80] W. S. M. Werner, C. Tomastik, T. Cabela, G. Richter, H. Störi, *J. Electron. Spectrosc. Relat. Phenom.* **2001**, *113*, 127.
[81] H. Venghaus, *Phys. Stat. Solidi B* **1975**, *71*, 609.
[82] A. Jablonski, F. Salvat, C. J. Powell, *J. Phys. Chem. Ref. Data* **2004**, *33*, 409.
[83] D. Bote, F. Salvat, A. Jablonski, C. J. Powell, *J. Electron Spectrosc. Relat. Phenom.* **2009**, *175*, 41.
[84] M. P. Seah, I. S. Gilmore, S. J. Spencer, *Surf. Interface Anal.* **2001**, *31*, 778.
[85] M. P. Seah, S. J. Spencer, *Surf. Interface Anal.* **2005**, *37*, 731.
[86] C. J. Powell, A. Jablonski, *J. Electron Spectrosc. Relat. Phenom.* **2001**, *114–116*, 1139.
[87] A. Jablonski, C. J. Powell, *Surf. Sci. Rep.* **2002**, *47*, 33.

